The genetic interaction of *REVOLUTA* and *WRKY53* links plant development, senescence, and immune responses

Authors/Affiliations

Justine Bresson[1,2#a*], Jasmin Doll[1], François Vasseur[2,3], Mark Stahl[1], Edda von Roepenack-Lahaye[1], Joachim Kilian[1], Bettina Stadelhofer[1], James M. Kremer[4,5#b], Dagmar Kolb[1], Stephan Wenkel[6] and Ulrike Zentgraf[1*]

[1]ZMBP, General Genetics, University of Tübingen, Tübingen, Germany
[2#a]CEFE, Univ Montpellier, CNRS, EPHE, IRD, Univ Paul Valéry Montpellier
[3]INRAE, Montpellier, France[3]LEPSE, Univ Montpellier, INRAE, Institut Agro, Montpellier, France
[4]Department of Microbiology and Molecular Genetics, Michigan State University, East Lansing, USA
[5#b]Joyn Bio, Boston, Massachusetts, USA
[6]Department of Plant and Environmental Sciences, University of Copenhagen, Frederiksberg C, Denmark

[*]***Corresponding authors***

j.bresson34@gmail.com (JB)

ulrike.zentgraf@zmbp.uni-tuebingen.de (UZ)

Date of submission: 22/06/2021
Number of tables and figures: 6 figures
Supporting data: 4 tables, 4 figures and Supplemental Methods

Abstract

In annual plants, tight coordination of successive developmental events is of primary importance to optimize performance under fluctuating environmental conditions. The recent finding of the genetic interaction of *WRKY53*, a key senescence-related gene with *REVOLUTA*, a master regulator of early leaf patterning, raises the question of how early and late developmental events are connected. Here, we investigated the developmental and metabolic consequences of an alteration of the *REVOLUTA* and *WRKY53* gene expression, from seedling to fruiting. Our results show that *REVOLUTA* critically controls late developmental phases and reproduction while inversely *WRKY53* determines vegetative growth at early developmental stages. We further show that these regulators of distinct developmental phases frequently, but not continuously, interact throughout ontogeny and demonstrated that their genetic interaction is mediated by the salicylic acid (SA). Moreover, we showed that *REVOLUTA* and *WRKY53* are keys regulatory nodes of development and plant immunity thought their role in SA metabolic pathways, which also highlights the role of *REV* in pathogen defence. Together, our findings demonstrate how late and early developmental events are tightly intertwined by molecular hubs. These hubs interact with each other throughout ontogeny, and participate to the interplay between plant development and immunity.

Introduction

The life cycle of flowering plants can be considered as a series of distinct growth phases driven by developmental genetic programs that integrate both environmental and endogenous stimuli. In annual plants, leaf senescence, defined as the last developmental stage, is often considered as an essential trait of plant adaptation to its biotic and abiotic environment [1]. Leaf senescence is

notably of utmost importance in the crosstalk between developmental, abiotic stress and immune responses, and influences plant productivity and fitness, as well as resistance to pathogens [2]. However, how senescence-related genes connect plant development, abiotic stress and immune responses still remains unclear. Moreover, this raises questions how early and late developmental events are coordinated by molecular hubs expressed throughout the life cycle.

The onset, progression and completion of leaf senescence are tightly regulated and depend on both plant age and growth environment. The senescence process occurs in an orderly manner, and without exogenous stress it mainly depends on the integration of age information at leaf and whole-plant levels [3]. In *Arabidopsis thaliana*, senescence is initiated as soon as full expansion of the leaves is reached and usually coincides with the transition from vegetative to reproductive growth [4]. During senescence progression, sequential changes arise coordinately in plant physiology and metabolism, and so implicate a large variety of genes involved for examples in the regulation of hormone, sugar and reactive oxygen species (ROS) levels [5]. The network of senescence-related genes initiates a well-orchestrated degradation of chlorophyll and other macromolecules, resulting in a sharp decrease of leaf photosynthetic activity [6]. When all essential nutrients have been remobilized to reach the reproductive parts of the plant, leaf death occurs as terminal phase of senescence [5,7].

Even though senescence is developmentally programmed, it can be strongly modulated by various exogenous factors. Stress, such as water stress or pathogen attack, can for example induce premature senescence as exit strategy to guarantee offspring under long-lasting unfavourable conditions [5]. Altogether, senescence is the result of a balance between developmental and environmental clues, integrating major transcriptional changes. In the case of pathogen infection, immune responses are induced and interfere with age-induced senescence

70 signals, which can, in some cases, lead to a precocious senescence [2]. Interestingly, large-scale
71 analyses of gene expression in senescing leaves of *A. thaliana* revealed that defence-related
72 genes represent a significant portion of the leaf senescence transcriptome [8]. Indeed, it has been
73 shown that their respective signalling pathways greatly overlap and several senescence-
74 associated genes (SAGs) are activated during both development and defence [8,9]. A large
75 fraction of the genes that operate at the nexus of development and defence encode proteins
76 involved in hormonal signalling. For instance, jasmonic (JA) and salicylic (SA) acids have long
77 been recognized as key hormones in the interconnection between age- and stress-induced
78 senescence [10]. JA, SA as well abscisic acid (ABA) levels increase during age-related
79 senescence [6] and signalling mutants are impaired in senescence onset and/or progression [11–
80 13].

81 Transcription factors (TF) also play a pivotal role as they often act as regulatory nodes between
82 signalling pathways and thus contribute to the fine-tuning of developmental and defence
83 responses [2]. Among the most relevant TFs, the *WRKY* gene family constitutes the second
84 largest group of the senescence transcriptome [14] and several *WRKYs* are also implicated in
85 plant immunity [15]. Consistently, *WRKY53* acts at a convergence point between age-induced
86 and stress-induced senescence [16,17]. For instance, *WRKY53* is known to be a positive regulator
87 of senescence initiation and interacts with a large number of genes involved in senescence
88 signalling, including other *WRKY* members and various SAGs [17,18]. Moreover, *WRKY53* has
89 been shown to be an important component of defence signalling pathways in Arabidopsis [16].
90 Dual functionality in plant immunity was observed: while *wrky53* mutant plants had increased
91 susceptibility toward *Pseudomonas syringae* [19,20], delayed symptoms were displayed during
92 *Ralstonia solanacearum* infection [21].

Owing to its key multi-function, *WRKY53* expression is under a complex control. Its expression is notably modulated by the cellular redox state, SA and JA. Its activity can be modulated by phosphorylation by a mitogen-activated protein kinase kinase kinase (MEKK1) or by interaction with *EPITHIOSPECIFYING SENESCENCE REGULATOR* (*ESR/ESP*), which both have functions in pathogen responses [22,23]. Recently, *REVOLUTA* (*REV*), a member of the class III homeodomain leucine zipper (*HD-ZIPIII*) TF family, has been identified as a direct and positive regulator of *WRKY53* expression [24]. *REV* is known to have pleiotropic effects during plant development [25]. It mainly regulates polarity associated-growth processes during early leaf development but also controls the formation of floral meristems [26,27]. REV is part of a regulatory network of HD-ZIPIII factors, miRNAs and microProteins [27–29]. Interestingly, an additional role for *REV* in late leaf development has been recently reported since loss-of-function mutations in *REV* strongly delayed the onset of senescence, through the control of the expression of *WRKY53* and other SAGs like e.g. *MORE AXILLARY BRANCHES 2* (*MAX2*) by the REV protein [24,30]. This result pointed out the importance of *REV* in the genetic control of age-induced senescence. However, despite its key role in senescence initiation, the implication of the *REV-WRKY53* genetic interaction through plant life cycle and immunity remains unknown.

In this paper, we examined whether the genetic interaction between *REV* and *WRKY53* occurs from early to late development phases, and controls plant metabolism and immune responses. Combining ecophysiological, metabolic and molecular analyses, we examined the role of *REV* and *WRKY53* in the dynamics of *A. thaliana* growth and responses to pathogen attack. This study was conducted using four mutants affected in *REV* and/or *WRKY53* expression, which allow deciphering the specific role of each gene and their combined roles. Our results showed that although *WRKY53* is a regulator of late leaf development, it also determined vegetative growth

evens at early developmental stages. Inversely, *REV* critically controlled late developmental phases and reproduction although it is known as a master regulator of early plant development and leaf patterning. Their genetic interaction fluctuated throughout ontogeny and dependent on environmental clues. Moreover, we showed that the *REVOLUTA-WRKY53* interaction is a key regulatory node of plant development and immunity through its role in SA metabolic pathways.

Results

REV and *WRKY53* control metabolic changes during senescence, especially related to SA metabolism

Senescence was dynamically analysed from flowering (first flower opens) until later developmental stages, ending with fruit ripening (first yellowing mature siliques) in wild-type plants (Col-0) as well as in four different mutants affected in *REV* and/or *WRKY53* expression: the mutants *rev5*, *wrky53* and *wrky53rev5* present single and double knock-out mutations [22,24], whereas *rev10-d* is a semi-dominant gain-of-function *REV* allele [27]. In all tested mutants, senescence was delayed after flowering, with a significant and strong deceleration 10 days after flowering, compared to Col-0 wild-type (Fig 1). In *rev5*, *wrky53* and *wrky53rev5* mutants, this delay was mainly due to postponed initiation of senescence in the first (oldest) leaves of the rosette (leaf position 1-8; S1 Fig). At later stages, the knock-out mutants reached similar percentages of senescent areas to Col-0, whereas *rev10-d* mutants were significantly less senescent until fruit ripening (*i.e.*, mature silique stage; Fig 1). This strong delayed senescence in *rev10-d* was the result of a higher number of younger healthy leaves and not a delay in the onset of senescence (leaf position 16-20; S1 Fig).

Fig 1. Analysis of senescence progression in the different *REV* and *WRKY53* mutants. Percentage of senescent area throughout the development from flowering to mature silique using chlorophyll fluorescence imaging. Senescent area was calculated by the ratio between pixel number for a photosynthetic efficiency $F_v/F_m \leq 0.6$ and the total pixel number of the rosette. Flowering was reached when the first flower was open. Mature silique stage was considered from the first yellowing siliques. Data are means (± SE) of 5-30 plants per genotype. Significant differences were analysed using Kruskal–Wallis tests: *: $P \leq 0.05$, **: $P \leq 0.001$, and ***: $P \leq 0.0001$. See also S1 Fig.

To understand whether and how *REV* and *WRKY53* influence plant metabolism during senescence progression, we measured 22 metabolites from flowering until mature silique stage, including phytohormones, and related components, sugars, amino and organic acids. The heat map of response ratio between Col-0 and mutants, revealed that the hierarchical clustering of the different conditions (*i.e.*, combining mutant and developmental stage) was not driven exclusively by plant development or by genotype but by a mixture between both (Fig 2A). At flowering, *rev5*, *wrky53* and *wrky53rev5* presented globally lower variations of response ratios (*i.e.* light colours) compared to *rev10-d* which presented a strong contrasting pattern, in which the majority of metabolites were found to be down-regulated, especially sugars and hormones (IAA, ABA, JA and SA-related components). The strongest observed dissimilarity in the response ratio of the mutants was found 15 days after flowering, while *rev5* at flowering was closely clustered to *rev10-d* at mature silique stage (Fig 2A). Throughout development, the double mutant *wrky53rev5* presented different patterns: it was closely clustered to *wrky53* at flowering and 5 days after flowering whereas it was more similar to *rev5* for the later stages.

Fig 2. Metabolite patterns in *REV* and *WRKY53* mutants over development. (A) Heat map analysis of metabolites in *REV* and *WRKY53* mutants compared to wild-type Col-0. The row represents metabolites and the column displays the different genotype-stage combinations. The colour scale indicates the values

of response ratio, calculated between the average of log-transformed values of Col-0 and a mutant at a given stage. Metabolite decreased is displayed in red, while metabolite increased is displayed in blue. White colour indicates no difference. The brightness of each colour corresponds to the magnitude of difference in the response ratio. The dendrogram represents the proximity between each genotype-stage metabolic pattern, as calculated from a hierarchical clustering analysis using Manhattan distance measures and Ward's hierarchical clustering method. **(B)** Principal component analysis on metabolite abundance values at 15 days after flowering. **Top**: representation of metabolites on the two first principal components. **Bottom**: projection of individual plants with centres of gravity per genotype (n=5). See also Tables S1-S2 and S2 Fig. IAA = auxin, ABA = abscisic acid, JA = jasmonic acid, SA = salicylic acid, SA bound = total SA after hydrolysis - free SA, SA conjugates = SA-(C6)-glycosides, DHBA = dihydroxybenzoic acid; DHBA bound = Total DHBA after hydrolysis - free DHBA; F = flowering; d = days and S = mature silique stage.

The differences in the metabolic patterns of mutants compared to Col-0 at 15 days after flowering were analysed through a PCA of metabolites (Fig 2B; S1 Table). PC1, which accounted for 30.4 % of the total variance, was strongly explained by camalexin content, which is a phytoalexin involved in plant responses to pathogen infection and is linked to ROS and SA signalling [31]. PC1 was secondly explained by SA, ABA, malate and JA contents. Variations along PC1 were mainly driven by *rev5* and *wrky53rev5* genotypes ($P < 0.01$; ANOVA on PC coordinates), which exhibited lower contents of these metabolites compared to Col-0 (S2 A-E Figs), as illustrated by their respective distance from the centroid of Col-0 (Fig 2B, S1 Table). PC2, which accounted for 20.1 % of the total variance, was mainly explained by SA-related components, such as dihydroxybenzoic acid (DHBA)-xylose and DHBA-bound (total DHBA after hydrolyses - free DHBA), which are main SA catabolites in Arabidopsis [32] but also SA-conjugates (SA-(C6)-glycosides) and SA-bound (total SA after hydrolyses – free SA). Variations

along PC2 were mainly driven by *rev10-d*, which presented the most significant genotypic effect ($P < 0.01$; ANOVA on PC coordinates; Fig 2B; S1 Table). Consistently, *rev10-d* displayed significant ($P < 0.01$) lower SA-conjugates and DHBA-xylose compared to Col-0 (S2 F-G Figs). Amongst all genotypes, *wrky53* displayed the least metabolic changes at 15 days after flowering compared to Col-0 (Fig 2B and S2 Fig). The analysis of the double mutant in senescing plants, by two-way ANOVA revealed an additive effect of *REV* and *WRKY53* mutations on SA and SA-related compound contents (S2 Table).

The salicylic acid signalling pathway is interconnected to *REV* and *WRKY53* genes

In view of metabolic changes occurring in the mutants, we explored how *REV, WRKKY53*, and SA metabolism could be linked.

We first evaluated the modifications of the SA signalling pathway in the *REV* and *WRKY53* mutants through two key genes in SA biosynthesis and catabolism (Figs 3A-B). The *ISOCHORISMATE SYNTHASE 1* (*ICS1;* also known as *SALICYLIC ACID INDUCTION DEFICIENT 2*, *SID2*) gene, which is involved in SA biosynthetic process [33], presented an increasing expression during senescence progression in Col-0 (Figs 1 and 3A). This up-regulation was significantly reduced in *wrky53rev5* upon 5 days after flowering compared to Col-0, whereas *rev5* and *rev10-d* had a strong reduction at 15 days after flowering (Fig 3A). In contrast, *wrky53* did not show any significant difference in *ICS1* expression over time. The expression of the *SA 3-HYDROXYLASE* (*S3H*; also named *SAG108*) gene which is involved in SA catabolism [34], exhibited similar trends as per *ICS1*. The expression of the *S3H* gene in Col-0 was increased during senescence and expression in all mutants tended to be lower at 15 days after flowering, with a significant effect for *wrky53* and *rev5* (Fig 3B).

Fig 3. Genetic regulation of SA-related genes and promoter activities of *REV* and *WRKY53* after salicylic acid treatments. Gene expression analysis by qRT-PCR over development: (**A**) *ICS1* and (**B**) *S3H*. qRT-PCR was performed in leaf at position 10, pooled by 5 per genotype per stage. Transcriptional levels were calculated based on the comparative $\Delta\Delta C_T$ method and normalized to *ACTIN2* levels. Data are means (±SE) of 2 biological replicates with 1–2 technical replicates. (**C**) GUS activities *in planta* after SA treatment. p*WRKY53*::GUS lines in Col-0 and *rev5* background, and p*REV*::GUS plants in *rev9* knock-out mutant [24,33],were used to quantify promoter activities. Data are means (± SE) of 2 biological and 2 technical replicates: 6-13 plants per genotype per condition. Significant differences were analysed using Kruskal–Wallis tests (*: $P \leq 0.05$; **: $P \leq 0.01$). See also S4 Table.

While the biosynthesis and catabolism of SA appears to be modulated by *REV* and *WRKY53* (Figs 3A-C), it has also been shown that *WRKY53* expression can be activated by exogenous SA in wild-type plants [22]. To identify whether *REV* expression is also regulated by SA and whether *REV* is involved in SA -induced expression of *WRKY53*, we made quantitative measurements of β-glucuronidase (GUS) activity *in planta* using both *REV* and *WRKY53* GUS-reporter lines after SA treatments. As expected, 19 h after SA-spraying on p*W53*::GUS rosettes, *WRKY53* expression was clearly induced. These results were modified when p*W53*::GUS was expressed in the *rev5* background (Fig 3C). Indeed, *WRKY53* expression in this line was weaker and no longer significantly induced by SA when comparing to p*W53*::GUS line with wild-type REV. This demonstrates that the hormonal regulation of *WRKY53* expression is modulated through the transcriptional factor REV. Moreover, our GUS expression analyses using p*REV*::GUS plants indicate that *REV* expression itself was not affected by SA treatments (Fig 3C).

The *REV-WRKY53* interaction controls early and late events of plant development from leaf production to fruit ripening

We performed a comprehensive analysis of plant development from germination to late developmental stages including specific hallmarks such as bolting (flower bud emergence), flowering and mature siliques.

The multivariate effects of the *REV-WRKY53* genetic interaction were first analysed through a principal component analysis (PCA) performed on 14 growth-related traits (S3 Table). First and second principal components (PCs) explained 40.2 % and 32.8 % of the total variance, respectively (S3 Fig). Projection of individuals revealed high genotypic variability as indicated by the distance of the genotypes from the centroid of each other. PC1 was mainly explained by the number and dry mass (DM) of leaves, flowering time and rate of leaf production (RLP; S3 Table), PC2 was driven by senescence- and fitness-related traits, such as the senescent area, reproductive allocation (calculated as the ratio between total silique and rosette DM) and stem size (S3 Table).

Throughout their life cycle, the different mutants exhibited contrasting growth trajectories (Fig 4A). The *rev10-d* gain-of-function and and the *rev5* loss-of-function mutant showed antagonistic growth strategies and presented opposite effects in RLP, total leaf number, flowering time and rosette DM (Figs 4A-D). In addition, *rev10-d* presented a faster and longer production of leaves, with a delayed flowering time compared to Col-0. As a result, *rev10-d* had a higher rosette DM. By contrast, *rev5* displayed a reduced RLP_{max}, less leaves, a precocious flowering time and thus a lower rosette DM compared to Col-0 (Figs 4A-D). While *rev10-d* and *rev5* had opposite phenotypes, *wrky53* mutant plants presented similar phenotypes as *rev5* but with a less pronounced effects: although *wrky53* tented to have a higher RLP_{max}, it presented a significant lower total leaf number, and less days to reach flowering compared to Col-0. The *wrky53rev5* double mutant displayed similar trends as *rev5* and *wrky53* but with an intermediate phenotype

(Figs 4A-D). During fruit ripening, the reproductive allocation was also greatly affected by *REV* and *WRKY53* expression; *wrky53* presented a significantly higher production of siliques per rosette DM than Col-0 whereas *rev10-d*, *rev5* and *wrky53rev5* had lower values (Fig 4E). On the contrary, although *rev10-d* had a much bigger rosette DM, this mutant produced less DM of siliques per rosette DM (Figs 4E-F).

Fig 4. Developmental analysis of the different *REV* and *WRKY53* mutants. **(A)** Rate of leaf production (RLP) during days after germination. Leaf number was counted from the two first true leaves until bolting. Insert in **A** represents the maximum RLP calculated as the slope (leaf per day), estimated by fitting a linear curve for each plant over time. **(B)** Leaf number at flowering. **(C)** Time to reach flowering. **(D)** Rosette dry mass at bolting. **(E)** Reproductive allocation at mature silique stage, calculated by the ratio of total silique dry mass per rosette dry mass. **(F)** A representative picture of rosettes and reproductive organs of the different genotypes at the mature silique. Bolting was defined by the emergence of the flower buds. Flowering was reached when the first flower was open and mature silique stage was considered from the first yellowing siliques. Data are means (± SE) of 5-30 plants per genotype. The different letters indicate significant differences following Kruskal–Wallis tests ($P \leq 0.05$). See also S2 and S3 Tables.

The analysis of the *REV-WRKY53* genetic interaction over the development revealed an interactive effect of the *REV* and *WRKY53* mutations on leaf number, flowering time, rosette DM, and a marginally significant effect on senescence at 10 days after flowering and reproductive allocation (results of two-way ANOVA; S2 Table).

REV and *WRKY53* mediate plant responses to pathogen

Because SA metabolism as well as camalexin production were altered in *wrky53* and *rev* mutants and a general overlap of senescence-associated and pathogen-associated genes has been reported,

we aimed to examine pathogen response in the mutants compared to wild-type plants. To explore the crosstalk between the *REV-WRKY53* interaction and plant immunity, we analysed the phenotypic responses to pathogen infection at early developmental stages. For all genotypes, 16-day-old rosettes (without visual senescence symptoms) were infected by spraying a suspension of a genetically modified strain of *Pseudomonas syringae* pv *tomato* DC3000 (*Pst*) constitutively expressing green fluorescent proteins (GFP), that allowed us to monitor its quantification in leaves (Fig 5A). In addition, plant susceptibility was followed after infection using chlorophyll fluorescence (ChlF) imaging through photosynthetic efficiency (F_v/F_m) measurements of whole-rosettes (Fig 5A). Response ratio of F_v/F_m, calculated as the relative ratio of *Pst*-infected plants compared to mock-treated plants, showed that 2 days after infection (DAI) *wrky53* and *rev5* tended to be more sensitive to the infection compared to Col-0, whereas *wrky53rev5* presented a significantly intensified sensitivity (Fig 5B). On the opposite, *rev-10d* appeared to be less sensitive than the others mutants and had a faster recovery of photosynthetic capacities, as illustrated by a reduced response ratio of F_v/F_m at 6 DAI when comparing to Col-0 (Fig 5B). Investigation of bacterial growth through GFP quantification at 14 DAI indicated that *wrky53rev5* had an increased colonisation of *Pst* in leaves (Fig 5C). These findings were confirmed by independent experiments (S4 Fig) but also through classical *Pst* bacterial leaf infiltration assays with subsequent bacterial growth curve evaluation (Fig 5D). Results of two-way ANOVA at 4 DAI revealed a strong additive effect of *REV* and *WRKY53* mutations ($P < 0.001$ and $P < 0.01$, respectively) on the susceptibility to *Pst* infection (*via* bacterial quantification, Fig 5D, S2 Table).

Fig 5. Pathogen assays using *Pseudomonas syringae* inoculation. 16-day-old plants were infected with *Pseudomonas syringae* (*Pst*) pv *tomato* DC3000, constitutively expressing GFP by spraying a *Pst*

suspension on leaf surfaces. Bacterial colonisation was followed by quantification of GFP fluorescence *in planta* and plant disease was investigated using chlorophyll fluorescence imaging. **(A) top**: a representative picture of rosettes 6 days after infection (DAI), in parallel to the respective mock condition. **Bottom**: a representation of GFP fluorencence *in planta* and photosynthetic efficiency (F_v/F_m) in *Pst*-infected plants 14 DAI **(B)** Response ratio of F_v/F_m during DAI, calculated as the relative ratio of *Pst*-infected plants compared to mock-treated plants (*Pst*-Mock)/Mock. Significant differences were analysed using two-way ANOVA (genotype by treatment interaction) on F_v/F_m values (n = 6-8; *:$P \leq 0.05$ and **:$P \leq 0.001$). **(C)** Quantification of bacterial growth *in planta* expressed in GFP units per rosette area compared to the respective mock condition, 14 DAI. Data are means (± SE) of 3 plants. **(D)** Quantification of bacterial growth after infection (cfu = colony forming units). Data are means (± SE) of 4-12 plants. Significant differences were analysed using Kruskal–Wallis tests (***: $P \leq 0.001$). See also S4 Fig.

REV and *WRKY53* connects plant growth, SA metabolism and immunity

The analyse of correlations amongst traits showed that RLP_{max}, flowering time, SA content and F_v/F_m response ratio after *Pst* infection, were all positively correlated (Fig 6). For instance, RLP_{max} and flowering time were highly correlated ($r^2 = 0.94$; $P \leq 0.05$), as well as SA content with F_v/F_m response ratio ($r^2 = 0.95$; $P \leq 0.05$). Moreover, increased RLP_{max} and delayed flowering time explained 86% and 82% of the variation in SA content, respectively. Plant sensitivity to pathogen infection (*i.e.* F_v/F_m values) was also explained by developmental traits: 66% by RLP_{max} and 60% by flowering time. *rev10-d* presented an opposite behaviour compared to the knock-out mutants, in which *wrky53rev5* had an intermediate phenotype between *wkry53* and *rev5*.

Fig 6. Correlations amongst key traits of plant development and immunity. Pearson correlation coefficients within the different genotypes of key traits of plant development and immunity. RLP_{max} is the maximum rate of leaf production calculated as the slope estimated by fitting a linear curve for each plant over time. Salicylic acid (SA) and F_v/F_m response ratio were measured at 15 days after flowering and 6 days after inoculation, respectively. (*: $P \leq 0.05$, .: $P \leq 0.01$).

Discussion

The coordination of developmental programs throughout the life cycle of a plant is a central question of plant biology and phenotypic integration. In this study, we showed that the genetic interaction between *WRKY53*, a key senescence-related gene [17], and *REV*, which is known as a leaf patterning gene [35], contribute to the fine-tuning of plant development, immunity and senescence.

The WRKY family represents one of the most abundant groups of TFs involved in the control of senescence [36]. As many TFs, WRKY members are also key actors in integrating developmental processes and stress responses [15]. Consistently, different WRKYs have been shown to be pivotal in pathogen defence [16]. For instance, WRKY53 acts as a positive regulator of basal resistance against *Pseudomonas syringae* (*Pst*) [19,20]. However, the upstream regulation of WRKYs appears to be very complex and remains far from being completely understood. Here, we investigated the pleiotropic role of REV, because previous studies demonstrated that REV directly and positively regulates the expression of *WRKY53* [24]. Moreover, REV also binds to additional differentially expressed senescence-associated genes during leaf senescence [24,30], which suggests that this gene controls many aspects of plant development through its interaction with senescence-related genes. Consistently, we found that

346 the *REV-WRKY53* interaction controls several developmental traits: leaf production rate,
347 flowering time and senescence, which later determine the reproductive success of plants (*i.e.,*
348 biomass production and reproductive allocation). Interestingly, multivariate analysis of
349 developmental and senescence traits revealed that traits related to flowering time and vegetative
350 growth were strongly correlated, shaping the first dimension of phenotypic variation (*e.g.*, PC1
351 explained more than 40% of total phenotypic variance). This is consistent with previous analyses
352 of natural variability performed in *A. thaliana*, in which traits related to growth rate and life
353 cycle duration also represents the first axis of phenotypic variability [37]. By contrast, we found
354 that SAGs were correlated to fitness-related traits, such as stem length and DM, as well as
355 reproductive allocation. This suggests that senescence is a key process involved in the control
356 and efficiency of reproduction, and that its role on fecundity dominates the role of flowering time
357 or vegetative growth. *REV* mutants exhibited stronger effect on senescence and fitness traits than
358 *WRKY53* mutants, which were more variable along the first phenotypic dimension. Strikingly,
359 this finding reveals that *REV*, a gene known as a master regulator of early leaf patterning [26–
360 28], critically controls late developmental phases and reproduction while, inversely, *WRKY53*, a
361 gene known as a master regulator of late leaf development [38], determines vegetative growth
362 even at early developmental stages. This unanticipated result demonstrates how late and early
363 developmental events are tightly intertwined by molecular hubs that interact with each other.

364 Moreover, our study revealed that the plant´s metabolism during growth was modified by *REV*
365 and *WRKY53*. Amongst the studied metabolites, SA and its related components were the most
366 variable ones between the mutants and Col-0. The analysis of the interaction between *REV* and
367 *WRKY53* by two-way ANOVA indicated that both genes were independently involved in SA-
368 related metabolic changes, and with a stronger effect of *REV*. By contrast, *REV* and *WRKY53*

exhibited significant interaction in the control of plant development, notably for total leaf number at reproduction, flowering time and shoot dry mass. In addition, *REV* and *WRKY53* exhibited no or marginal interaction in the control of senescence and fitness traits. Taken together, our results suggest that REV and WRKY53 strongly interact during plant development, while they later act independently in the control of senescence through the SA signalling pathway.

Since we found that the biosynthesis as well as catabolism of SA can be modulated by *REV* and *WRKY53*, SA-related gene expression was analysed. Two SA biosynthetic pathways have been characterized in plants, the phenylalanine ammonia lyase (PAL) pathway and the isochorismate (IC) pathway, both using chorismite as primary metabolite. However, approx. 90% of the SA produced after pathogen attack or UV light exposure are produced via the IC pathway [39,40]. Isochorismate synthase (ICS) and isochorismate pyruvate lyase can convert chorismate to SA via isochorismate. Moreover, SA can also be stored in form of inactive SA glycosides (SA 2-O-β-D-glucose and SA glucose ester) which are actively transported to the vacuole and can be converted back to SA [41,42]. 2,3- and 2,5-dihydroxybenzoic acid (2,3-DHBA and 2,5-DHBA) sugar conjugates appear to be the major storage form in vacuoles of old Arabidopsis leaves [32,43] and SA 3-hydroxylase (S3H), which converts SA to 2,3-DHBA, prevents over-accumulation of active SA implying an important role in regulating leaf senescence [32]. Consistent with previous findings [42], we showed that the expression of the *S3H* gene increased in senescing leaves of wild-type Col-0 plants. However, this up-regulation was damped in the mutants, with a significant interaction of *REV* and *WRKY53* mutations. In addition, we found that *ICS1* expression is also diminished in the mutants compared to the senescence-associated increase in wild-type, with a strong decrease in *rev10-d*. Thus, the control of isochorismate synthase and SA

3-hydroxylase activity by the *REV-WRKY53* interaction is expected to be crucial for the fine-tuning of plant senescence.

However, SA is known as a multifaceted hormone which is also of utmost importance for disease resistance, but also for flowering and senescence [44,45]. Through its effect on the SA signalling pathway, the *REV-WRKY53* interaction could be a key driver of the already described growth-defence trade-off [10]. In order to test this hypothesis, we sprayed plant seedlings with *Pst* to test the response of *REV* and *WRKY53* mutants to pathogen attack. Since *Pst* enters the plant through natural openings or wounds, this method just mimicked their natural entry into the apoplastic space [46]. Interestingly, we observed improved resistance against these pathogens in *rev1*0-*d* compared to Col-0, although this mutant grew faster and higher than the wild-type. This suggests that the behaviour and phenotype of *rev10-d* can be explained by a higher SA content but also by a faster and longer production (*i.e.,* delayed flowering) of healthy leaves after infection. In addition, not only SA metabolism but also the production of camalexin, which appears to be the major phytoalexin involved in biotic responses in *A. thaliana* [31,46], is also altered in the mutants. Camalexin production exhibited the same pattern as free SA, most likely contributing to the resistance of *rev10-d.*

Moreover, we have shown that the induction of *WRKY53* expression by SA is dependent on REV as SA induction of a *WRKY53* promoter driven GUS reporter gene was severely impaired in the *rev* mutant background. However, *REV* expression appeared to be insensitive to SA, which means that there is a feed-back loop of SA production to *WRKY53* expression but not to REV expression. In the same line of evidence, REV is also involved in the response of *WRKY53* expression by H_2O_2 [24] and SA induces the accumulation of H_2O_2, and *vice versa*. On the other

hand, the DNA-binding activity of the REV protein is redox-sensitive indicating a very complex feed-back regulation between *REV*, *WRKY53*, H_2O_2 and SA.

Collectively, our results indicate that the genetic interaction between *REV* and *WRKY53* seems to be strongly dependent on the developmental stage and that *REV* acts upstream of *WRKY53* to modulate SA signalling from early to late plant development.

Materials and Methods

Plant material and growth conditions

The *A. thaliana* ecotype Col-0 and the following mutants in the Col-0 background were used in this study: *rev5*, (A260V) a strong ethyl-methylsulfonate (EMS) allele of *REV* ; *wrky53*, (SALK-034157) a T-DNA insertion line in the second exon of *WRKY53* [22]; *wrky53rev5*, a double knock-out mutant [24] and *rev10-d*, a semi-dominant gain-of-function of *REV* allele where *REV* mRNA was rendered resistant to the negative regulation by microRNAs [27]. p*WRKY53*::GUS lines in Col-0 and *rev5* background, and p*REV*::GUS plants in *rev9* knock-out mutant [24,35] were used to quantify promoter activity *in planta*. Plants were grown on standard soil (9:1 soil and sand) under controlled conditions: in long days (16 h day; 8 h night), low light (~70-80 µE m^{-2} s^{-1} at plant height) and an ambient temperature of 21 °C (see [47] for details). Three independent experiments were done for developmental analysis, including senescence and plant productivity quantification.

Plant developmental analysis

The number of leaves that were visible to the naked eye (at least/minimum of 2-3 mm) was counted every day to determine the RLP from the emergence of the first two true leaves until macroscopic visualization of flower buds (bolting). The maximum RLP was determined as the

436 slope estimated by fitting a linear curve for each plant over time. Bolting, flowering time and
437 mature silique were determined as the number of days from germination until bolting, the first
438 flower open and the first yellowing siliques, respectively. At each stage, plants were individually
439 harvested and leaf blades were separated from their petiole considering the position (age) within
440 the rosette. Leaf blades were scanned for measurements of area using the ImageJ software
441 (1.47v, Rasband, Bethesda, Maryland, USA). The maximum rate of leaf expansion (R_{max}) was
442 determined as for [49]. Specific leaf area (SLA) was calculated as the ratio of total leaf area to
443 leaf DM. DM of the different organs (leaves, petioles and stems) was measured by placing them
444 in separate paper bags at 67 °C for at least 5 days.

445 ## Senescence and plant productivity quantification

446 Due to significant differences in phenology of mutants, senescence progression was analysed
447 from the first flower open for each individual plant. Senescence was quantified in leaves using
448 ChlF imaging (Imaging-PAM; Maxi version; ver. 2-46i, Heinz Walz GmbH; see [47,48]). The
449 maximum quantum yield of photosystem II (PSII) was estimated by the ratio of variable to
450 maximal ChlF (F_v/F_m, also called photosynthetic efficiency) on dark-adapted plants, after 15-20
451 min. Senescent area was estimated by a clustering approach of F_v/F_m values of each pixel of the
452 ChlF image (according to [49]). Senescent area was calculated by the ratio between pixel number
453 for $F_v/F_m \leq 0.6$ and the total pixel number of the rosette (or in single leaves). Silique number was
454 counted at mature silique stage and siliques were dried in a paper bag at 67 °C for at least 5 days.
455 Reproductive allocation was calculated by the ratio of total silique DM per rosette DM.

456 ## Metabolomics analysis: extraction of primary and secondary
457 ## metabolites

For each genotype and senescence stage 5 replica samples were created. For each replica, leaves at position 5 to 11 were po-oled and weighed for each plant from flowering to mature silique stages. 10 mg of freeze dried, retched (5 mm steel ball; 30 sec) plant material was extracted with 200 µl 80 % methanol (MeOH; 0.1 % formic acid (FA); ice cold). The pellet was re-extracted with 200 µl 20 % MeOH (0.1 % FA; icecold) and both supernatants were combined. The whole extraction process was done at 10 °C including a 10 min sonication and centrifugation step (18600 g). For the analysis of the free and conjugated phytohormones the final extract was directly used for targeted liquid chromatography–mass spectrometry (LC-MS) analysis (see Supplemental methods). To determine the amount of bound SA and DHBA, 50 µl of the plant extracts were hydrolyzed with 4 µl concentrated FA (99 °C; 2 h; 800 rpm), cooled down on ice and centrifuged (10 °C; 18600 g) before submitting them into the targeted LC-MS pipeline. For the analysis of sugars and amino acids, 100 µl extracts were dried down in a speed vacum concentrator before derivatisation for gas chromatography-MS (GC-MS) analysis (see Supplemental methods). For non-targeted LC-MS analysis, the same extraction was performed as for the targeted approach (see Supplemental methods). The combined supernatants from the extraction were dried down in a speed vacum concentrator and afterwards redissolved in 100 µl 20 % MeOH containing 0,1 % FA and 9 µM L-Encephalin as an internal standard. In addition 10 µl of each sample was combined to create a pool sample of the entire analysis. 5 µl of any sample were injected for the non-targeted LC-MS analysis.

Gene expression analysis

In two independent experiments (same growth conditions as above), gene expression levels were followed by qRT-PCR according to [48]. Leaves at position 10 were harvested from flowering to mature silique stages in individual plants. A pool of 5 leaves per genotype/stage was used for

RNA extraction and cDNA synthesis. Samples harvested at mature silique stage were removed from the analyses because very low amounts of RNA could be isolated and no reliable transcript levels were detected. Transcriptional changes were calculated based on the comparative $\Delta\Delta C_T$ method [50] and normalized to *ACTIN2* levels. Primers used are listed in S4 Table.

Quantitative measurement of GUS activity *in planta* after SA treatments

Two-week-old plants were used to analyse GUS activity *in planta* by spraying whole-rosette with 2 mM SA in 0.15 % ethanol and 0.02 % Silwet L-77. Control plants were treated using appropriate mock solution. GUS activity was measured according to [51]. Rosettes were individually frozen in liquid nitrogen, homogenized using Mill MM 200 (Retsch GmbH, Germany) and resuspended in 1 mL GUS Extraction Buffer (50 mM sodium phosphate pH 7.0, 10 mM EDTA, 10 mM β-mercaptoethanol, 0.1 % triton X-100, 0.1 % sarcosyl and 25 µg ml^{-1} PMSF). Samples were strongly vortexed and centrifuged at 13.000 rpm for 15 min at room temperature. 200 µL of supernatant were then kept on ice. 10 µL of extracts were added in 130 µL Assay Buffer (GUS Extraction Buffer containing 2 mM 4-methylumbelliferyl β-D-glucuronide; MUG). After 20 min at 37 °C, 10 µL of the reaction were transferred to 190 µL of a 200 mM sodium carbonate solution in a 96-well dark plate. Fluorescence was measured on a TriStar LB941 plate reader (Berthold Technologies, Germany) at 460 nm (emission) and 355 nm (excitation). A standard curve from 0 to 50 µM of 4-methylumbelliferone (4-MU) was used to calculate moles of MU min^{-1} produced after the cleavage of MUG by GUS enzyme in *planta*. 2 µL of extracts in 200 µL of 5-fold diluted Bradford Roti-Quant (Roth, Germany) were used to quantify protein concentration of samples [52] and to calculate the final GUS activity in nmol MU min^{-1} mg^{-1}.

Pathogen assays and bacterial quantification

Pathogen assays were performed using *Pst* pv *tomato* DC3000 *att*Tn*7*-egfpmut3 constitutively expressing GFP. *Pst* pv *tomato* DC3000 was labeled via Tn*7* site-specific transposition with the mini-Tn*7* vector pURR25 [53] essentially as described in [54]. Bacteria were grown overnight at 28 °C in dark in specific medium (1 % (w/v) tryptone, 0.6 % (w/v) yeast extract, 0.15 % (w/v) K_2HPO_4, 0.06 % (w/v) NaCl, pH 7) supplemented with rifampicin (50 µg mL^{-1}) and kanamycin (25 µg mL^{-1}) to OD_{600} = 0.8. The inoculum preparation and Arabidopsis infection were then done as described by Katagiri et al., (2002). A final density of $5x10^8$ colony-forming unit mL^{-1} (cfu mL^{-1}) of bacterial suspension, in sterile water with 0.02 % (v/v) Silwet L-77, was used for spray inoculation of 16-day-old plants. As control, a mock solution (0.02 % (v/v) Silwet L-77 in sterile water) was used. Inoculation was done twice (8h intervals) and plants were kept covered with a transparent plastic lid for 2 days. Bacterial colonisation was analysed by quantifying GFP fluorescence in abaxial leaf surface using a Typhoon FLA9500 laser scanner (GE Healthcare) and ImageJ analysis. Plant disease was followed after the infection using ChlF imaging through F_v/F_m measurements of whole-rosettes, as described above. A response ratio of F_v/F_m was calculated as the relative ratio of *Pst*-infected plants compared to mock-treated plants followed (*Pst*-Mock)/Mock. In independent experiments, *Pst* pv *tomato* DC3000, grown overnight at 28 °C to OD_{600} = 0.2 in King's B medium supplemented with 50µg mL^{-1} of rifampicin, was infiltrated at a density of $1x10^4$ cfu mL^{-1} in 10 mM $MgCl_2$ in leaf tissue with a needleless syringe. Middle age leaves (fourth or fifth leaves from young to old) of 6-week-old plants, grown under short day conditions, were used for infiltration. Bacterial growth (cfu cm^2) was measured in two discs per leaf after extracting bacteria. For this purpose, leaf discs were incubated in 70 % ethanol for 1 min, dried on filter paper, subsequently washed briefly washing in water for 1 min,

again dried on filter paper and then homogenized in 200 µL of 10 mM $MgCl_2$. Subsequent serial dilutions and depositions on LB-plates with 50 µg mL^{-1} of cycloheximide and 50 µg mL^{-1} of rifampicin were performed by using multichannel pipettes.

Statistical analyses

PCAs were performed on developmental or metabolite values to focus on genotypic effects at a given developmental stage [55]. *REV* and *WRKY53* mutation effects were analysed in analyses of variance (ANOVA) on PC coordinates. Metabolite patterns (heat map) of mutants were analysed using response ratio, calculated between log-transformed values of Col-0 and a mutant at a given stage. A hierarchal cluster diagram was constructed using Manhattan distances and Ward's hierarchical clustering method. Comparisons of mean trait values between genotypes were performed using Kruskal–Wallis nonparametric tests for developmental analysis. All analyses were performed using R software (3.4.3 v.; R Development Core Team, 2012).

Accession numbers

Sequence data from this article can be found in the GenBank/EMBL data libraries under the following accession numbers: *ACTIN2* (At3g18780), *ICS1* (*SID2*; At1g74710), *REV* (At5g60690), *S3H* (*SAG108*; At4g10500), *WRKY53* (At4g23810).

Acknowledgment

We thank Manuela Freund, Julian Fratte and Gesine Seibold for their technical support. We thank Brian H. Kvitko and Emanuele Scacchi for providing us the line of *Pseudomonas syringae* pv *tomato* DC3000 attTn7-egfpmut3 constitutively expressing GFP.

Author Contributions

J.B. designed the research, performed experiments, analyzed the data, wrote the manuscript and secured funding. U.Z. designed, supervised the research, wrote the manuscript and secured funding. S.W. designed, supervised the research, contributed to writing and secured funding. J.D. performed qRT-PCRs for gene expression analysis, and contributed to writing. F.V. wrote the manuscript. M.S., E.v.R.L., J.K. and B.S. performed metabolite quantification. J.M.K. designed and provided the line of *Pseudomonas syringae* pv *tomato* DC3000 *att*Tn*7*-egfpmut3 constitutively expressing GFP. D.K. performed bacterial leaf infiltration assays. All co-authors read and approved the final manuscript. JB was supported by the Institutional Strategy of the University of Tuebingen (Deutsche Forschungsgemeinschaft, ZUK 63) and also funded by the Alexander von Humboldt Foundation. This work was supported by the Deutsche Forschungsgemeinschaft (CRC1101, B06).

References

1. Wingler A, Purdy S, MacLean JA, Pourtau N. The role of sugars in integrating environmental signals during the regulation of leaf senescence. J Exp Bot. 2006;57: 391–399. doi:10.1093/jxb/eri279

2. Häffner E, Konietzki S, Diederichsen E. Keeping Control: The Role of Senescence and Development in Plant Pathogenesis and Defense. Plants. 2015;4: 449–488. doi:10.3390/plants4030449

3. Zentgraf U, Jobst J, Kolb D, Rentsch D. Senescence-Related Gene Expression Profiles of Rosette Leaves of Arabidopsis thaliana: Leaf Age Versus Plant Age. Plant Biol. 2004;6: 178–183. doi:10.1055/s-2004-815735

4. Thomas H. Senescence, ageing and death of the whole plant. New Phytol. 2013;197: 696–711. doi:10.1111/nph.12047

5. Lim PO, Kim HJ, Nam HG. Leaf Senescence. Annu Rev Plant Biol. 2007;58: 115–136. doi:10.1146/annurev.arplant.57.032905.105316

6. Breeze E, Harrison E, McHattie S, Hughes L, Hickman R, Hill C, et al. High-Resolution Temporal Profiling of Transcripts during Arabidopsis Leaf Senescence Reveals a Distinct Chronology of Processes and Regulation. Plant Cell. 2011;23: 873–894. doi:10.1105/tpc.111.083345

577 7. Havé M, Marmagne A, Chardon F, Masclaux-Daubresse C. Nitrogen remobilization during
578 leaf senescence: lessons from Arabidopsis to crops. J Exp Bot. 2017;68: 2513–2529.
579 doi:10.1093/jxb/erw365

580 8. Guo Y, Gan S. Convergence and divergence in gene expression profiles induced by leaf
581 senescence and 27 senescence-promoting hormonal, pathological and environmental stress
582 treatments. Plant Cell Environ. 2011;35: 644–655. doi:10.1111/j.1365-3040.2011.02442.x

583 9. Quirino BF, Normanly J, Amasino RM. Diverse range of gene activity during Arabidopsis
584 thaliana leaf senescence includes pathogen-independent induction of defense-related genes. Plant
585 Mol Biol. 1999;40: 267–278. doi:10.1023/A:1006199932265

586 10. Huot B, Yao J, Montgomery BL, He SY. Growth–Defense Tradeoffs in Plants: A Balancing
587 Act to Optimize Fitness. Mol Plant. 2014;7: 1267–1287. doi:10.1093/mp/ssu049

588 11. Morris K, A. -H. -Mackerness S, Page T, John CF, Murphy AM, Carr JP, et al. Salicylic acid
589 has a role in regulating gene expression during leaf senescence. Plant J. 2000;23: 677–685.
590 doi:10.1046/j.1365-313x.2000.00836.x

591 12. Pourtau N, Marès M, Purdy S, Quentin N, Ruël A, Wingler A. Interactions of abscisic acid
592 and sugar signalling in the regulation of leaf senescence. Planta. 2004;219: 765–772.
593 doi:10.1007/s00425-004-1279-5

594 13. He Y, Fukushige H, Hildebrand DF, Gan S. Evidence Supporting a Role of Jasmonic Acid in
595 Arabidopsis Leaf Senescence. Plant Physiol. 2002;128: 876–884. doi:10.1104/pp.010843

596 14. Guo Y, Cai Z, Gan S. Transcriptome of Arabidopsis leaf senescence. Plant Cell Environ.
597 2004;27: 521–549. doi:10.1111/j.1365-3040.2003.01158.x

598 15. Eulgem T, Somssich IE. Networks of WRKY transcription factors in defense signaling. Curr
599 Opin Plant Biol. 2007;10: 366–371. doi:10.1016/j.pbi.2007.04.020

600 16. Pandey SP, Somssich IE. The Role of WRKY Transcription Factors in Plant Immunity. Plant
601 Physiol. 2009;150: 1648–1655. doi:10.1104/pp.109.138990

602 17. Zentgraf U, Laun T, Miao Y. The complex regulation of WRKY53 during leaf senescence of
603 Arabidopsis thaliana. Eur J Cell Biol. 2010;89: 133–137. doi:10.1016/j.ejcb.2009.10.014

604 18. Miao Y, Laun T, Zimmermann P, Zentgraf U. Targets of the WRKY53 transcription factor
605 and its role during leaf senescence in Arabidopsis. Plant Mol Biol. 2004;55: 853–867.
606 doi:10.1007/s11103-004-2142-6

607 19. Murray SL, Ingle RA, Petersen LN, Denby KJ. Basal Resistance Against Pseudomonas
608 syringae in Arabidopsis Involves WRKY53 and a Protein with Homology to a Nematode
609 Resistance Protein. Mol Plant Microbe Interact. 2007;20: 1431–1438. doi:10.1094/MPMI-20-11-
610 1431

611 20. Hu Y, Dong Q, Yu D. Arabidopsis WRKY46 coordinates with WRKY70 and WRKY53 in
612 basal resistance against pathogen Pseudomonas syringae. Plant Sci. 2012;185–186: 288–297.
613 doi:10.1016/j.plantsci.2011.12.003

614 21. Hu J, Barlet X, Deslandes L, Hirsch J, Feng DX, Somssich I, et al. Transcriptional
615 Responses of Arabidopsis thaliana during Wilt Disease Caused by the Soil-Borne
616 Phytopathogenic Bacterium, Ralstonia solanacearum. PLoS ONE. 2008;3.
617 doi:10.1371/journal.pone.0002589

618 22. Miao Y, Zentgraf U. The Antagonist Function of Arabidopsis WRKY53 and ESR/ESP in
619 Leaf Senescence Is Modulated by the Jasmonic and Salicylic Acid Equilibrium. Plant Cell.
620 2007;19: 819–830. doi:10.1105/tpc.106.042705

621 23. Miao Y, Laun TM, Smykowski A, Zentgraf U. Arabidopsis MEKK1 can take a short cut: it
622 can directly interact with senescence-related WRKY53 transcription factor on the protein level
623 and can bind to its promoter. Plant Mol Biol. 2007;65: 63–76. doi:10.1007/s11103-007-9198-z

624 24. Xie Y, Huhn K, Brandt R, Potschin M, Bieker S, Straub D, et al. REVOLUTA and
625 WRKY53 connect early and late leaf development in Arabidopsis. Development. 2014;141:
626 4772. doi:10.1242/dev.117689

627 25. Talbert PB, Adler HT, Parks DW, Comai L. The REVOLUTA gene is necessary for apical
628 meristem development and for limiting cell divisions in the leaves and stems of Arabidopsis
629 thaliana. Development. 1995;121: 2723–2735.

630 26. Otsuga D, DeGuzman B, Prigge MJ, Drews GN, Clark SE. REVOLUTA regulates meristem
631 initiation at lateral positions. Plant J Cell Mol Biol. 2001;25: 223–236. doi:10.1046/j.1365-
632 313x.2001.00959.x

633 27. Emery JF, Floyd SK, Alvarez J, Eshed Y, Hawker NP, Izhaki A, et al. Radial Patterning of
634 Arabidopsis Shoots by Class III HD-ZIP and KANADI Genes. Curr Biol. 2003;13: 1768–1774.
635 doi:10.1016/j.cub.2003.09.035

636 28. Juarez MT, Kui JS, Thomas J, Heller BA, Timmermans MCP. microRNA-mediated
637 repression of rolled leaf1 specifies maize leaf polarity. Nature. 2004;428: 84–88.
638 doi:10.1038/nature02363

639 29. Wenkel S, Emery J, Hou B-H, Evans MMS, Barton MK. A Feedback Regulatory Module
640 Formed by LITTLE ZIPPER and HD-ZIPIII Genes. Plant Cell. 2007;19: 3379–3390.
641 doi:10.1105/tpc.107.055772

642 30. Hong S-Y, Botterweg-Paredes E, Doll J, Eguen T, Blaakmeer A, Matton S, et al. Multi-level
643 analysis of the interactions between REVOLUTA and MORE AXILLARY BRANCHES 2 in
644 controlling plant development reveals parallel, independent and antagonistic functions.
645 Development. 2020;147. doi:10.1242/dev.183681

646 31. Glawischnig E. Camalexin. Phytochemistry. 2007;68: 401–406.
647 doi:10.1016/j.phytochem.2006.12.005

32. Zhang K, Halitschke R, Yin C, Liu C-J, Gan S-S. Salicylic acid 3-hydroxylase regulates Arabidopsis leaf longevity by mediating salicylic acid catabolism. Proc Natl Acad Sci U S A. 2013;110: 14807–14812. doi:10.1073/pnas.1302702110

33. Nawrath C, Métraux J-P. Salicylic Acid Induction–Deficient Mutants of Arabidopsis Express PR-2 and PR-5 and Accumulate High Levels of Camalexin after Pathogen Inoculation. Plant Cell. 1999;11: 1393–1404. doi:10.1105/tpc.11.8.1393

34. Gan S, Zhang K. Increasing leaf longevity and disease resistance by altering salicylic acid catabolism. US20160312239A1, 2016. Available: https://patents.google.com/patent/US20160312239A1/en

35. Brandt R, Salla-Martret M, Bou-Torrent J, Musielak T, Stahl M, Lanz C, et al. Genome-wide binding-site analysis of REVOLUTA reveals a link between leaf patterning and light-mediated growth responses. Plant J. 2012;72: 31–42. doi:10.1111/j.1365-313X.2012.05049.x

36. Rushton PJ, Somssich IE, Ringler P, Shen QJ. WRKY transcription factors. Trends Plant Sci. 2010;15: 247–258. doi:10.1016/j.tplants.2010.02.006

37. Vasseur F, Bontpart T, Dauzat M, Granier C, Vile D. Multivariate genetic analysis of plant responses to water deficit and high temperature revealed contrasting adaptive strategies. J Exp Bot. 2014;65: 6457–6469. doi:10.1093/jxb/eru364

38. Zentgraf U, Doll J. Arabidopsis WRKY53, a Node of Multi-Layer Regulation in the Network of Senescence. Plants. 2019;8: 578. doi:10.3390/plants8120578

39. Wildermuth MC, Dewdney J, Wu G, Ausubel FM. Isochorismate synthase is required to synthesize salicylic acid for plant defence. Nature. 2001;414: 562–565. doi:10.1038/35107108

40. Garcion C, Lohmann A, Lamodière E, Catinot J, Buchala A, Doermann P, et al. Characterization and Biological Function of the ISOCHORISMATE SYNTHASE2 Gene of Arabidopsis. Plant Physiol. 2008;147: 1279–1287. doi:10.1104/pp.108.119420

41. Dean JV, Mohammed LA, Fitzpatrick T. The formation, vacuolar localization, and tonoplast transport of salicylic acid glucose conjugates in tobacco cell suspension cultures. Planta. 2005;221: 287–296. doi:10.1007/s00425-004-1430-3

42. Vaca E, Behrens C, Theccanat T, Choe J-Y, Dean JV. Mechanistic differences in the uptake of salicylic acid glucose conjugates by vacuolar membrane-enriched vesicles isolated from Arabidopsis thaliana. Physiol Plant. 2017;161: 322–338. doi:10.1111/ppl.12602

43. Bartsch M, Bednarek P, Vivancos PD, Schneider B, Roepenack-Lahaye E von, Foyer CH, et al. Accumulation of Isochorismate-derived 2,3-Dihydroxybenzoic 3-O-β-d-Xyloside in Arabidopsis Resistance to Pathogens and Ageing of Leaves. J Biol Chem. 2010;285: 25654–25665. doi:10.1074/jbc.M109.092569

44. Rivas-San Vicente M, Plasencia J. Salicylic acid beyond defence: its role in plant growth and development. J Exp Bot. 2011;62: 3321–3338. doi:10.1093/jxb/err031

684 45. Wasternack C, Hause B. Jasmonates: biosynthesis, perception, signal transduction and action
685 in plant stress response, growth and development. An update to the 2007 review in Annals of
686 Botany. Ann Bot. 2013;111: 1021–1058. doi:10.1093/aob/mct067

687 46. Ausubel FM, Katagiri F, Mindrinos M, Glazebrook J. Use of Arabidopsis thaliana defense-
688 related mutants to dissect the plant response to pathogens. Proc Natl Acad Sci. 1995;92: 4189–
689 4196. doi:10.1073/pnas.92.10.4189

690 47. Bresson J, Bieker S, Riester L, Doll J, Zentgraf U. A guideline for leaf senescence analyses:
691 from quantification to physiological and molecular investigations. J Exp Bot. 2018;69: 769–786.
692 doi:10.1093/jxb/erx246

693 48. Bresson J, Vasseur F, Dauzat M, Koch G, Granier C, Vile D. Quantifying spatial
694 heterogeneity of chlorophyll fluorescence during plant growth and in response to water stress.
695 Plant Methods. 2015;11: 23. doi:10.1186/s13007-015-0067-5

696 49. Rousseau C, Belin E, Bove E, Rousseau D, Fabre F, Berruyer R, et al. High throughput
697 quantitative phenotyping of plant resistance using chlorophyll fluorescence image analysis. Plant
698 Methods. 2013;9: 17. doi:10.1186/1746-4811-9-17

699 50. Pfaffl MW. A new mathematical model for relative quantification in real-time RT–PCR.
700 Nucleic Acids Res. 2001;29: e45–e45. doi:10.1093/nar/29.9.e45

701 51. Francis KE, Spiker S. Identification of Arabidopsis thaliana transformants without selection
702 reveals a high occurrence of silenced T-DNA integrations. Plant J. 2005;41: 464–477.
703 doi:10.1111/j.1365-313X.2004.02312.x

704 52. Bradford MM. A rapid and sensitive method for the quantitation of microgram quantities of
705 protein utilizing the principle of protein-dye binding. Anal Biochem. 1976;72: 248–254.
706 doi:10.1016/0003-2697(76)90527-3

707 53. Teal TK, Lies DP, Wold BJ, Newman DK. Spatiometabolic stratification of Shewanella
708 oneidensis biofilms. Appl Environ Microbiol. 2006;72: 7324–7330. doi:10.1128/AEM.01163-06

709 54. Stice SP, Thao KK, Khang CH, Baltrus DA, Dutta B, Kvitko BH. Thiosulfinate Tolerance Is
710 a Virulence Strategy of an Atypical Bacterial Pathogen of Onion. Curr Biol. 2020;30: 3130-
711 3140.e6. doi:10.1016/j.cub.2020.05.092

712 55. Chessel D, Dufour AB, Thioulouse J. The ade4 package-I-One-table methods. R News.
713 2004;4: 5–10.

714

Supporting information

S1 Table. Loadings of the variables included in the PCA on mean of metabolite abundance values. Percentages indicate the percentage the total variance explained in the three first principal components (PC). Loadings are correlation coefficients between the variables and PCs. DM = dry mass

Trait (unit)	PC1	PC2	PC3
	30.4%	**20.1%**	**17.3%**
Camalexin (ng mg^{-1} DM)	0.87	-0.14	-0.23
Salicyl acid (SA; ng mg^{-1} DM)	0.86	0.062	-0.26
Acid abscisic (ABA; ng mg^{-1} DM)	0.86	0.11	-0.36
Malate (area mg^{-1} DM)	0.85	0.37	-0.16
Jasmonic Acid (JA; ng mg^{-1} DM)	0.73	-0.37	-0.42
Lactate (area mg^{-1} DM)	0.73	0.56	-0.19
Trehalose (ng mg^{-1} DM)	0.6	0.007	0.66
Glucose (ng mg^{-1} DM)	0.59	0.12	0.73
Auxin (IAA; pg mg^{-1} DM)	-0.57	-0.36	-0.095
Dihydroxybenzoic acid (DHBA; area mg^{-1} DM)	0.57	-0.57	-0.19
Sucrose (ng mg^{-1} DM)	0.51	-0.044	0.74
Fumarate (area mg^{-1} DM)	0.48	0.64	-0.22
Fructose (area mg^{-1} DM)	0.46	-0.11	0.81
SA bound (ng mg^{-1} DM)	0.39	-0.71	-0.013
Succinate (area mg^{-1} DM)	0.38	0.44	-0.15
Pyruvate (area mg^{-1} DM)	-0.33	0.43	-0.11
DHBA bound (area mg^{-1} DM)	0.28	-0.66	0.064
Citrate (area mg^{-1} DM)	-0.23	-0.015	-0.27
SA conjugates (area mg^{-1} DM)	0.13	-0.89	-0.094
DHBA xylose (area mg^{-1} DM)	0.13	-0.9	-0.12
Glutamine (ng mg^{-1} DM)	0.09	-0.0036	-0.64
Proline (ng mg^{-1} DM)	0.09	-0.02	-0.73

S2 Table. Coefficients of genetic interaction between *REV* and *WRKY53* on metabolic, developmental and immune traits. Two-way ANOVA performed on log_{10}-transformed values of developmental traits over the developement. ns = non significant, .: $P \leq 0.1$, *: $P \leq 0.05$, **: $P \leq 0.001$, and ***: $P \leq 0.0001$. B = bolting, F = flowering, F+10d = 10 days after flowering and S

724 = mature silique stage; SA bound = total SA after hydrolysis - free SA, SA conjugates = SA-
725 (C6)-glycosides, DHBA = dihydroxybenzoic acid; DHBA bound = Total DHBA after hydrolysis
726 - free DHBA; cfu = colony forming units

Trait	Intercept		*REV*WRKY53*	
Developmental analysis				
Rate of leaf production	-0.157	***	0.013	ns
Leaf number	1.140	***	0.055	**
Flowering time	1.555	***	0.029	*
Senescent area (F+10d)	1.158	***	0.482	.
Shoot dry mass (S)	-0.854	***	0.139	*
Reproductive allocation	-0.358	***	-0.206	.
Number Silique	1.883	***	-0.015	ns
Metabolic analysis				
SA	8.84	***	3.28	ns
SA bound	22.5	***	4.82	ns
SA conjugates	75556	**	-5610	ns
DHBA xylose	3902.6	**	140.4	ns
DHBA bound	265439	***	91354	ns
Pathogen assays				
log cfu cm-2	16.86	***	0.91	ns

727 **S3 Table. Loadings of the variables included in the PCA on mean of 14 growth-related**
728 **traits values.** Percentages indicate the percentage the total variance explained in the three first
729 principal components (PC). Loadings are correlation coefficients between the variables and PCs.

Trait (unit)	PC1	PC2	PC3
	40.2%	**32.8%**	**9.5%**
Leaf number (leaf)	-0.94	0.05	0.02
Leaf dry mass (g)	-0.94	0.08	0.25
Bolting time (d)	-0.86	-0.0039	0.14
Flowering time (d)	-0.85	-0.38	0.0062
Specific leaf area (SLA; $m^2\ g^{-1}$)	0.78	0.46	-0.23
Whole-rosette area (cm^2)	-0.76	0.5	0.14
Rate of leaf production (RLP; leaf d^{-1})	-0.74	0.04	-0.063
Maximum rate of leaf expansion (R_{max}; $cm^2\ d^{-1}$)	0.52	0.31	0.38
Senescent area (%)	-0.27	0.62	-0.68
Stem dry mass (g)	-0.23	0.85	0.29

Petiole dry mass (g)	-0.19	-0.85	-0.19
Stem lenght (cm)	-0.11	0.91	0.17
Reproductive allocation	0.26	0.9	0.18
Whole-rosette F_v/F_m	0.37	-0.64	0.62

S4 Table. List of primers used.

Gene	Locus	Direction	Primer Sequence
ACTIN2	At3g18780	Forward	ACCCGATGGGCAAGTCATCACG
		Reverse	TCCCACAAACGAGGGCTGGA
SAG13	At2g29350	Forward	AGGGAGCATCGTGCTCATATCC
		Reverse	CCAGCTGATTCATGGCTCCTTTG
S3H	At4g10500	Forward	AATATCGGCGACCAAATGCAGGTC
		Reverse	ACTACGGCTCTATGGAGCACAC
SID2	At1g74710	Forward	GCTTGGCTAGCACAGTTACAGC
		Reverse	CACTGCAGACACCTAATTGAGTCC

S1 Fig. Percentage of senescent area by leaf position of the different mutants compared to Col-0. (**A**) Percentage of senescent area displayed at 10 days and (**B**) 15 days after flowering. Senescent area was calculated by the ratio between pixel number for $F_v/F_m \leq 0.6$ and the total pixel number of the rosette. Black line means wild-type Col-0, colours show mutants. Data are means (± SE) of 5 plants.

S2 Fig. Abundances of main metabolites explaining the most significant effects in PCA at 15 days after flowering. (**A**) camalexin, (**B**) salicylic acid (SA), (**C**) abscisic acid (ABA), (**D**) malate, (**E**) jasmonic acid (JA), (**F**) dihydroxybenzoic acid (DHBA) xylose and (**G**) SA conjugates. Data are means (±SE) of 5 plants. Different letters indicate significant differences between means following Kruskal-Wallis tests ($P < 0.05$). DM = dry mass; SA conjugates = SA-(C6)-glycosides.

S3 Fig. Principal component analysis on multiple growth-related traits measured on *REV* and *WRKY53* mutants. (**A**) Representation of the variables, measured at 10 days after

744 flowering, on the two first principal components. DM = dry mass; RLP = rate of leaf production;
745 R_{max} = maximum rate of leaf expansion; SLA = specific leaf area; F_v/F_m = maximum quantum
746 yield of photosystem II. (**B**) Projection of individual plants with centres of gravity per genotype
747 (n = 5). Ellipses represent inertia ellipses, centred on the means for each genotype. Their width
748 and height are given by 1.5 times the standard deviation of the coordinates on axes, and the
749 covariance sets the slope of the main axis [58]. *rev5* and *wrky53* are single knock-out of the *REV*
750 and *WRKY53* genes, respectively. *wrky53rev5* is double knock-out (Xie et al., 2014). *rev10-d* a
751 semi-dominant gain-of-function of *REV* allele where *REV* mRNA is rendered resistant to the
752 negative regulation by microRNAs [27].

753 **S4 Fig. Pathogen assays.** 16-day-old plants were infected with *Pseudomonas syringae* (*Pst*) pv
754 *tomato* DC3000, constitutively expressing GFP by spraying a *Pst* suspension on leaf surfaces.
755 (**A**) Response ratio of photosynthetic efficiency (F_v/F_m) during days after infection (DAI),
756 calculated as the relative ratio of *Pst*-infected plants compared to mock-treated plants (*Pst*-
757 Mock)/Mock. **(B)** Quantification of bacterial growth *in planta* expressed in GFP units per rosette
758 area compared to the respective mock condition. Data are means (± SE) of 3-5 plants per
759 condition.

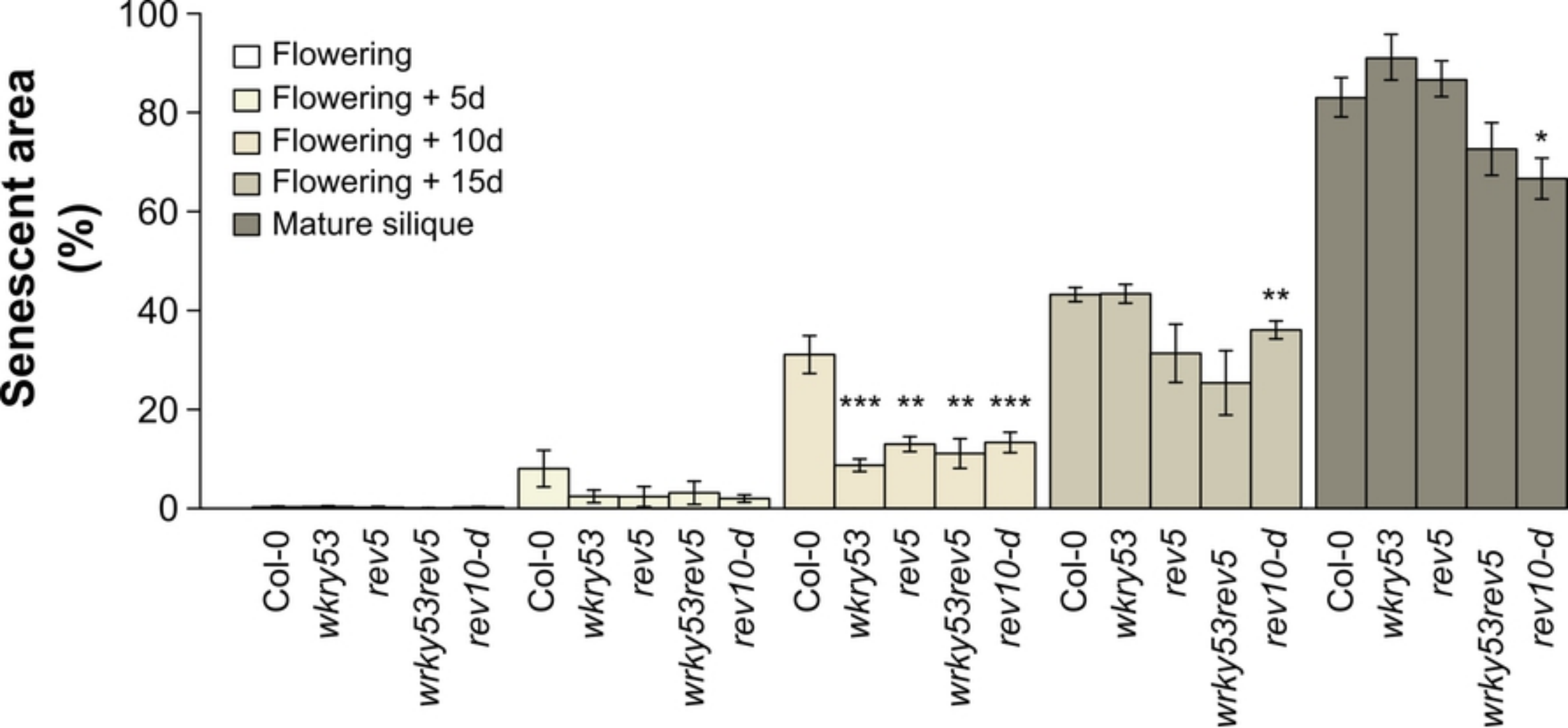
Senescent area (%)
100
80
60
40
20
0
Flowering
Flowering + 5d
Flowering + 10d
Flowering + 15d
Mature silique
***
**
**
***
**
*
Col-0
wkry53
rev5
wrky53rev5
rev10-d

Figure 1

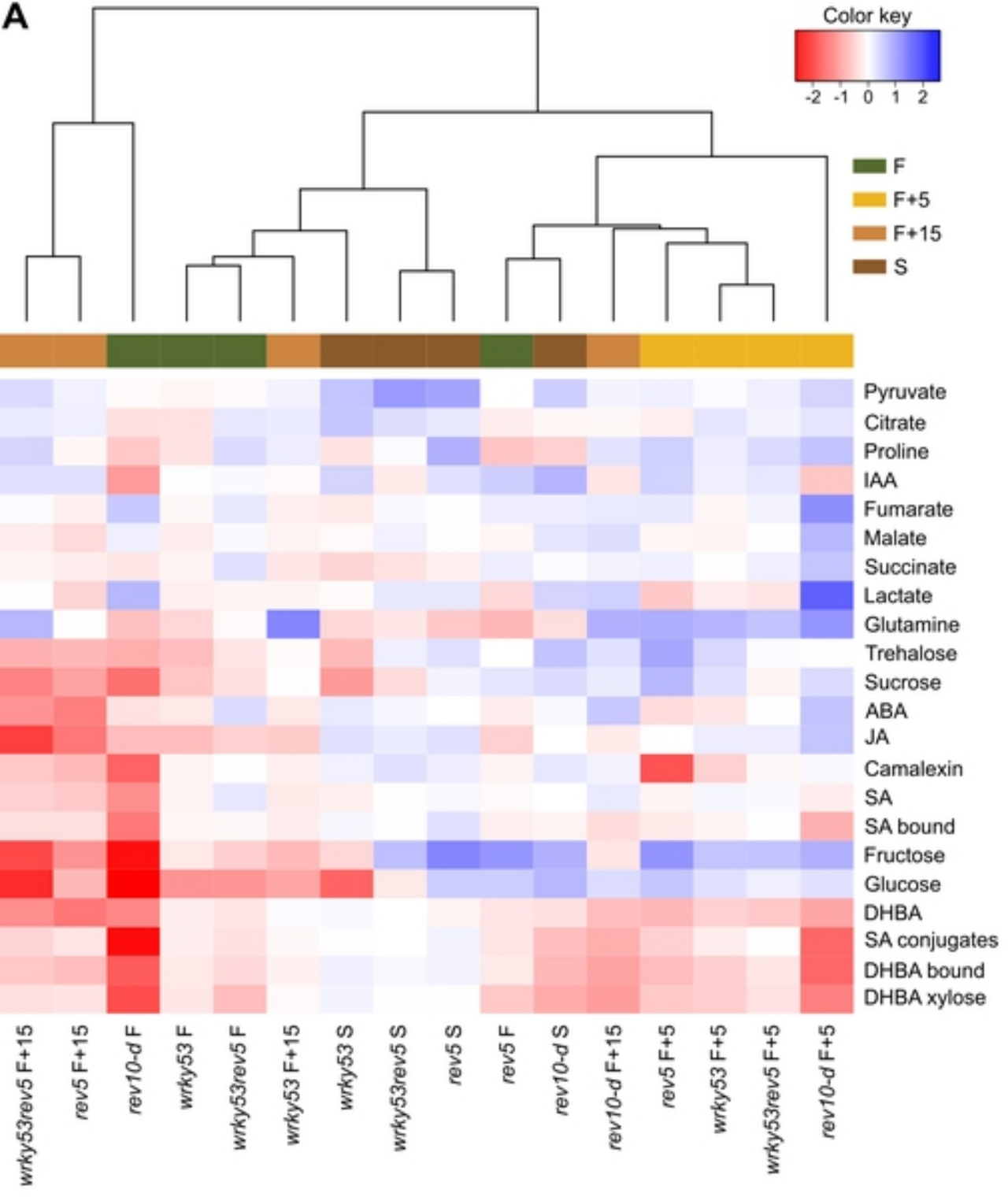
A
Color key
-2 -1 0 1 2
F
F+5
F+15
S
Pyruvate
Citrate
Proline
IAA
Fumarate
Malate
Succinate
Lactate
Glutamine
Trehalose
Sucrose
ABA
JA
Camalexin
SA
SA bound
Fructose
Glucose
DHBA
SA conjugates
DHBA bound
DHBA xylose
wrky53rev5 F+15
rev5 F+15
rev10-d F
wrky53 F
wrky53rev5 F
wrky53 F+15
wrky53 S
wrky53rev5 S
rev5 S
rev5 F
rev10-d S
rev10-d F+15
rev5 F+5
wrky53 F+5
wrky53rev5 F+5
rev10-d F+5

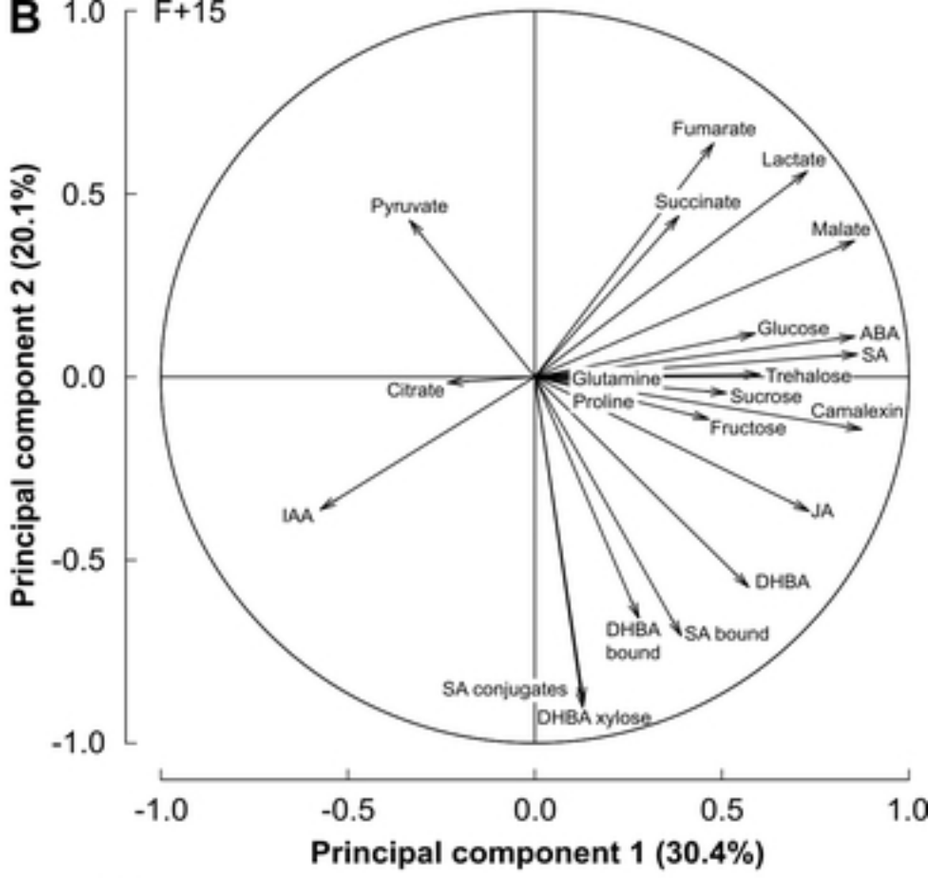
B
F+15
Principal component 2 (20.1%)
Principal component 1 (30.4%)
Fumarate
Lactate
Succinate
Malate
Pyruvate
Glucose
ABA
SA
Glutamine
Trehalose
Citrate
Proline
Sucrose
Camalexin
Fructose
JA
IAA
DHBA
DHBA bound
SA bound
SA conjugates
DHBA xylose

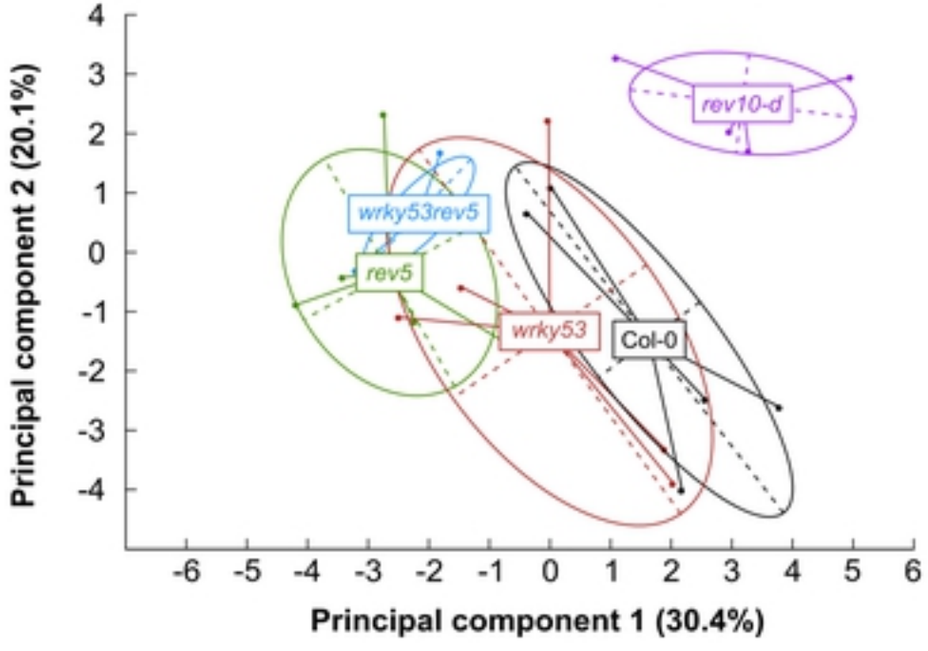
Principal component 2 (20.1%)
Principal component 1 (30.4%)
rev10-d
wrky53rev5
rev5
wrky53
Col-0

Figure 2

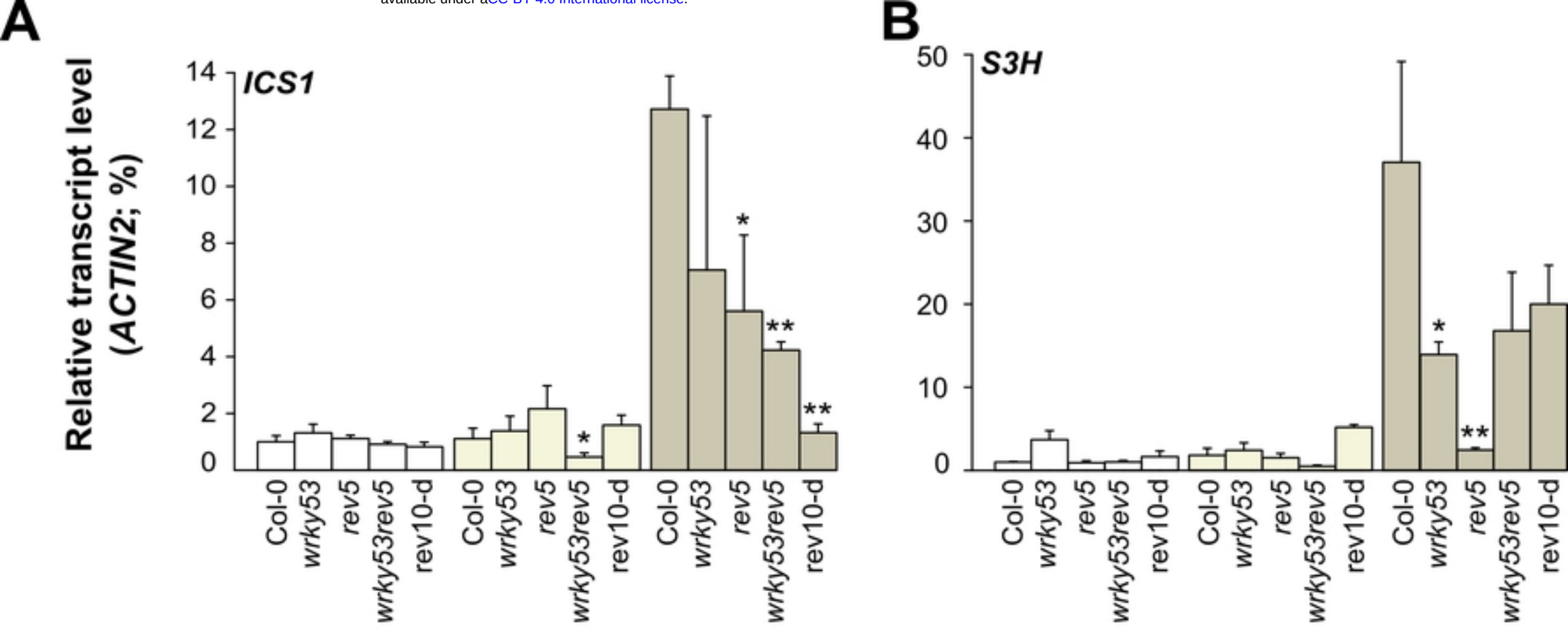

Figure 3

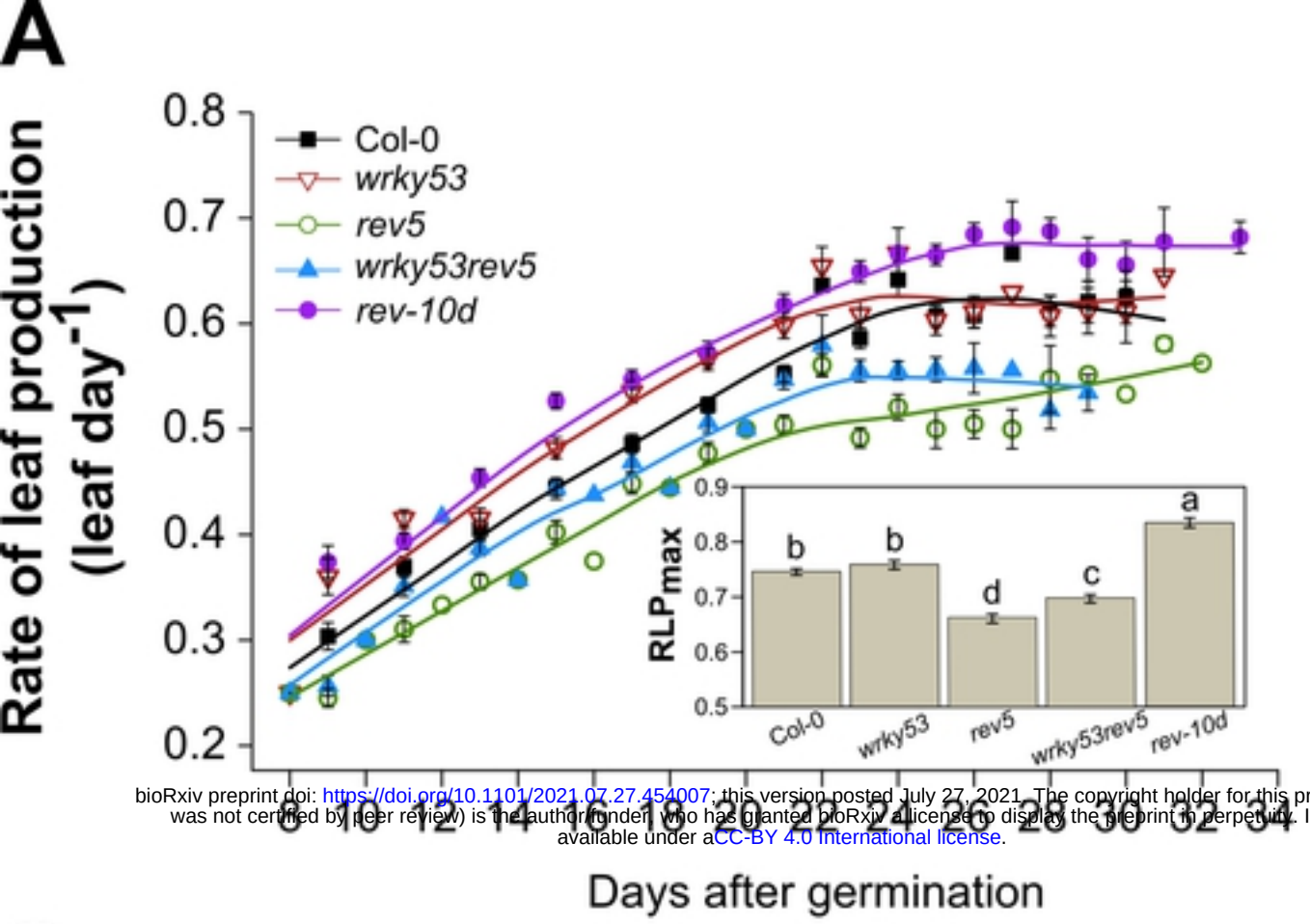

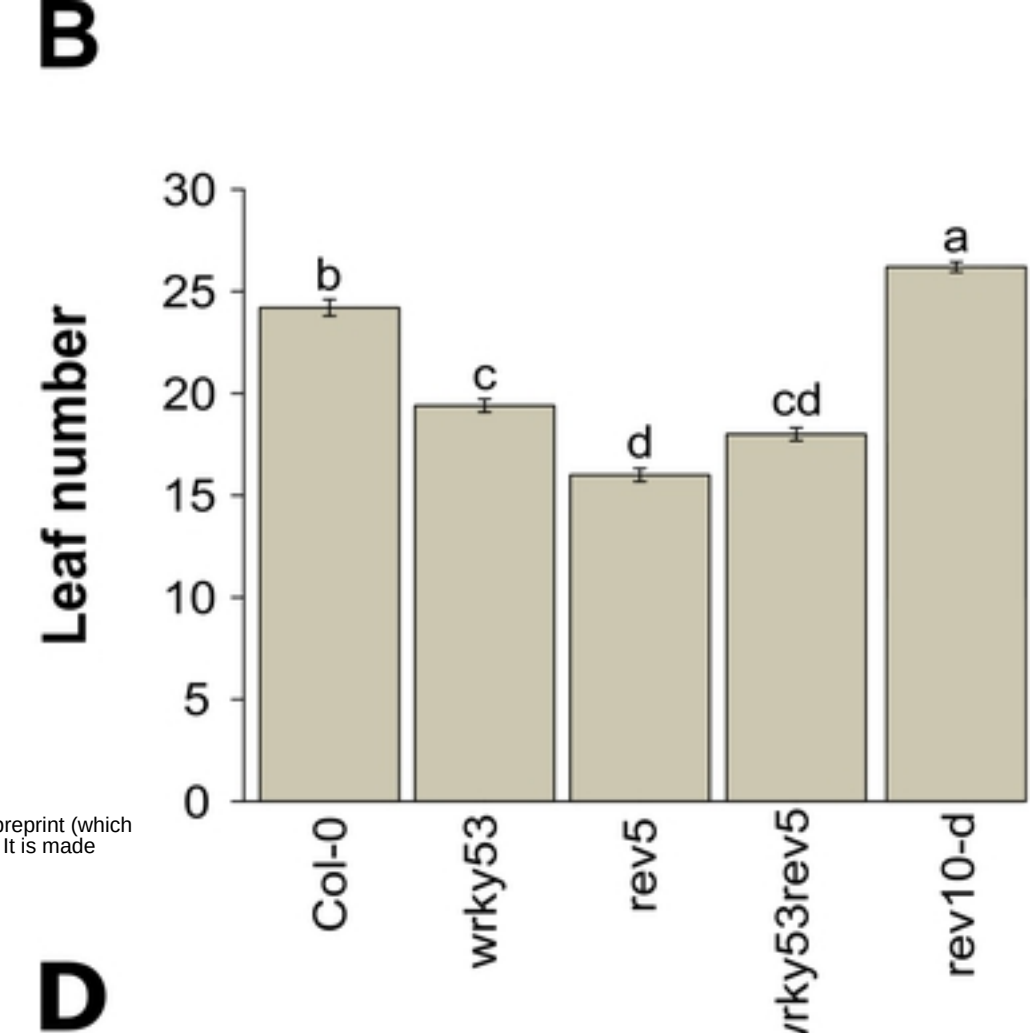

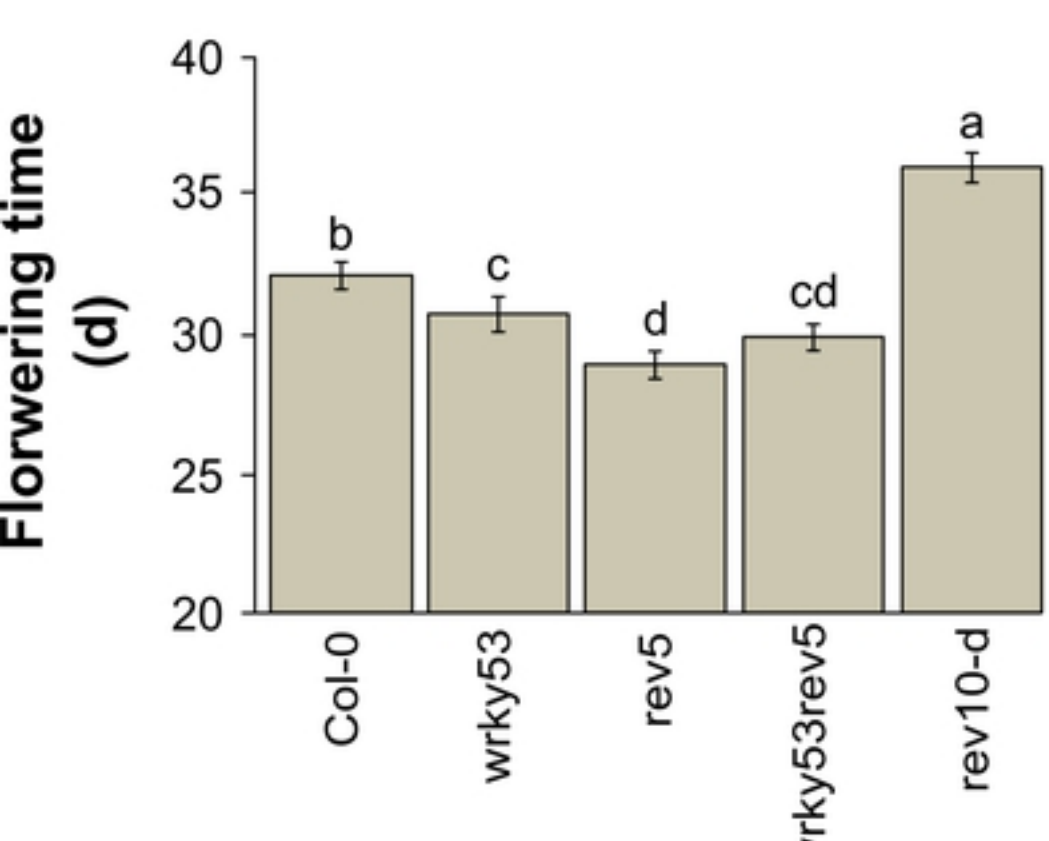

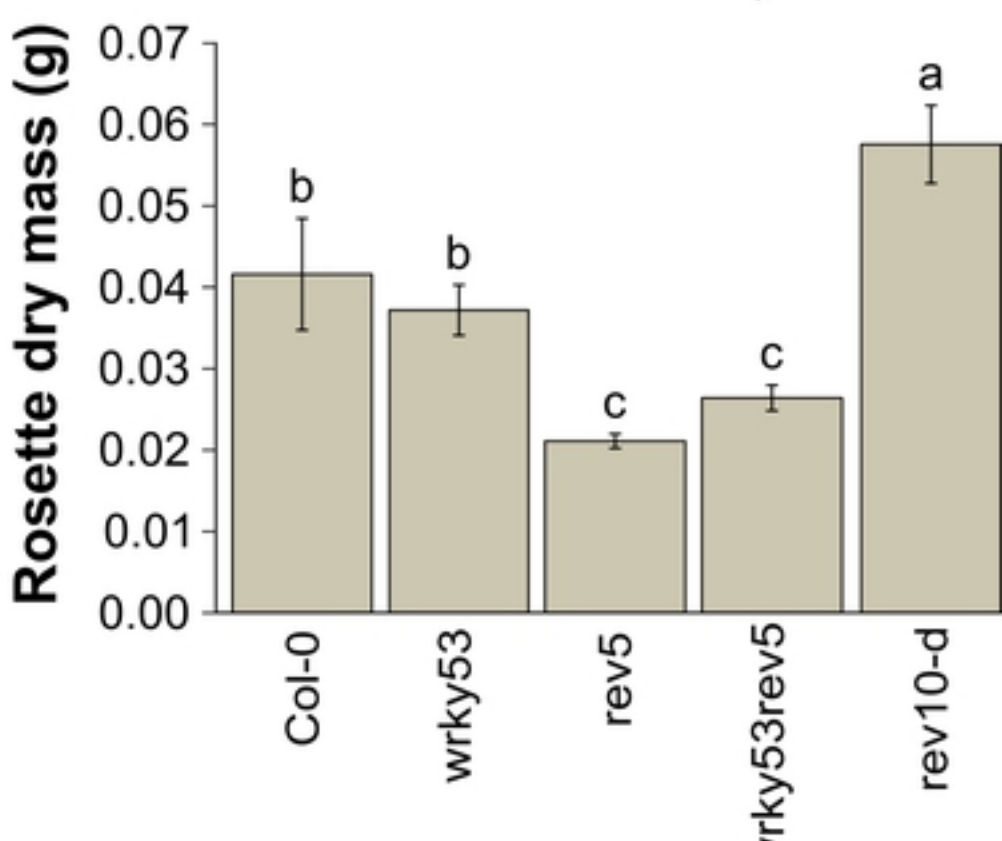

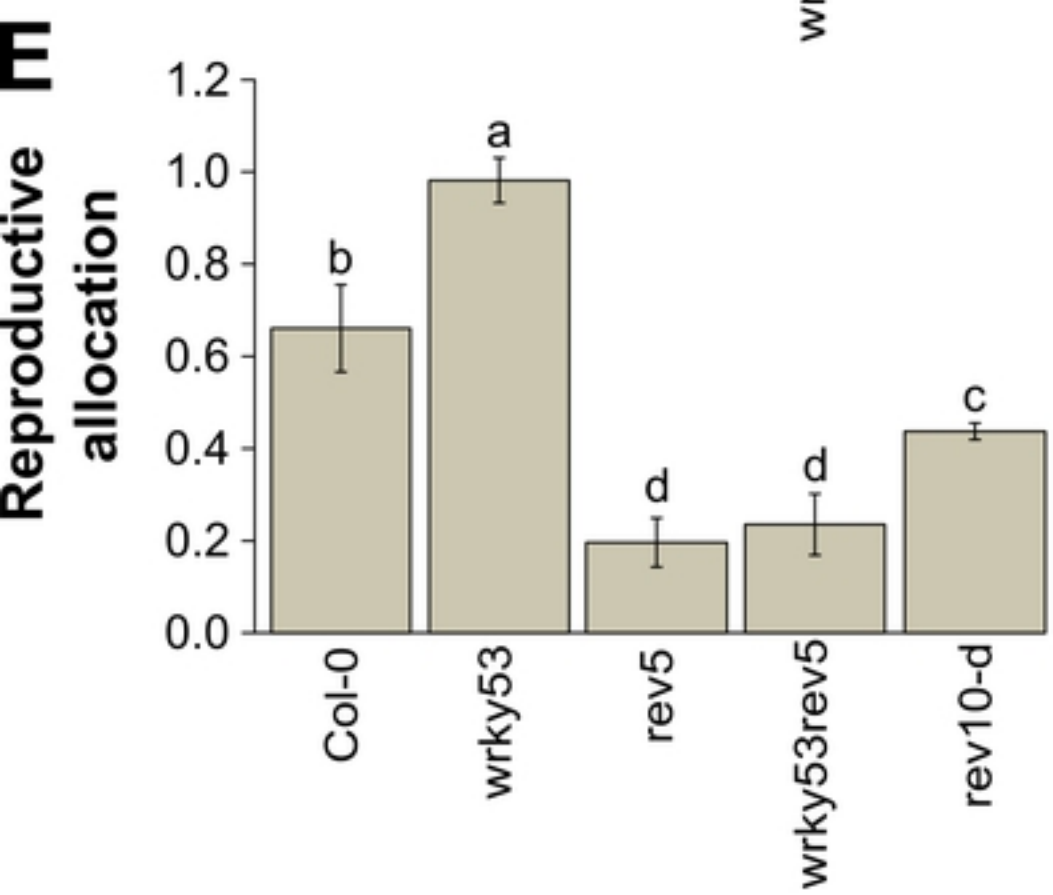

Figure 4

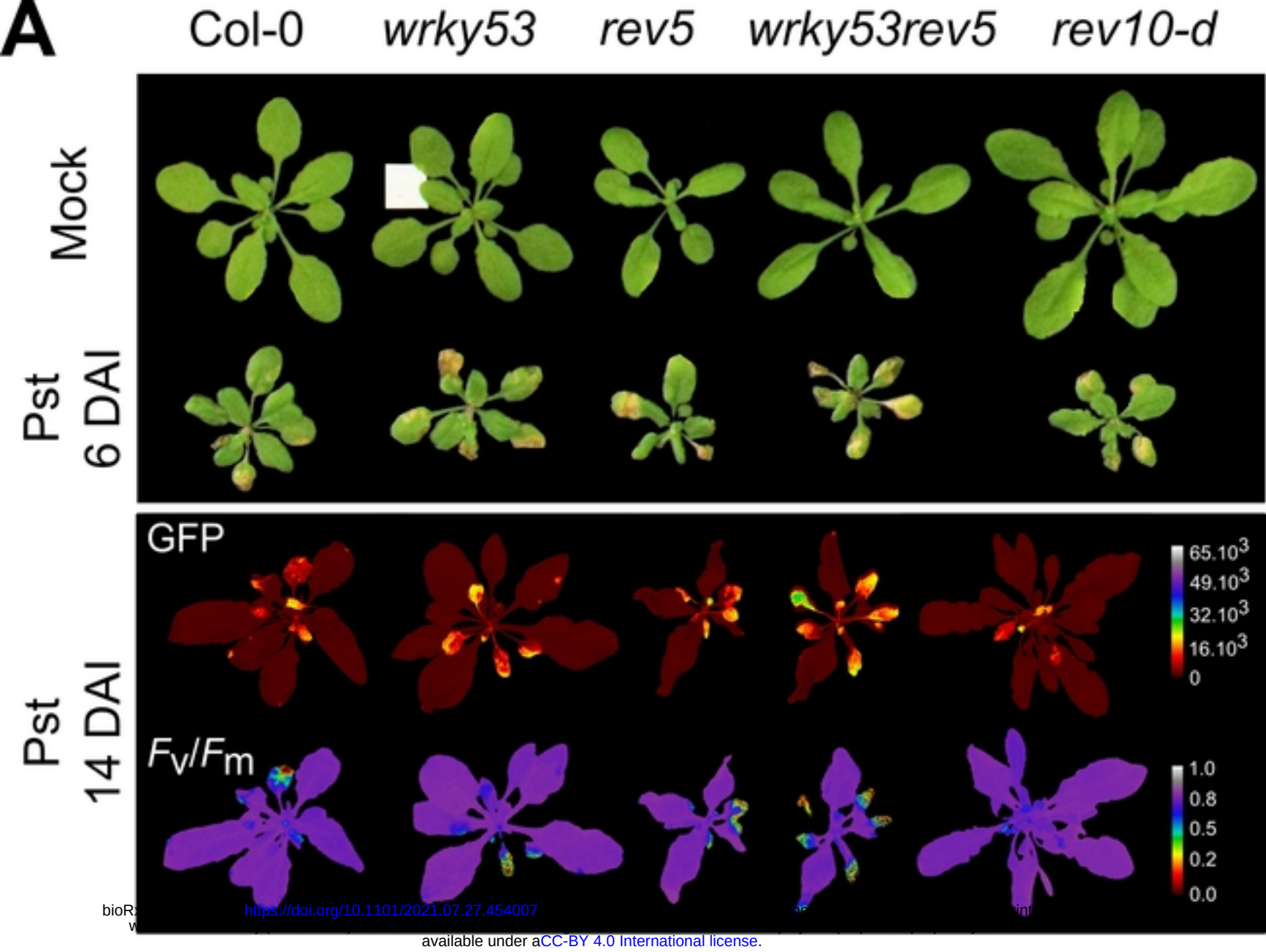

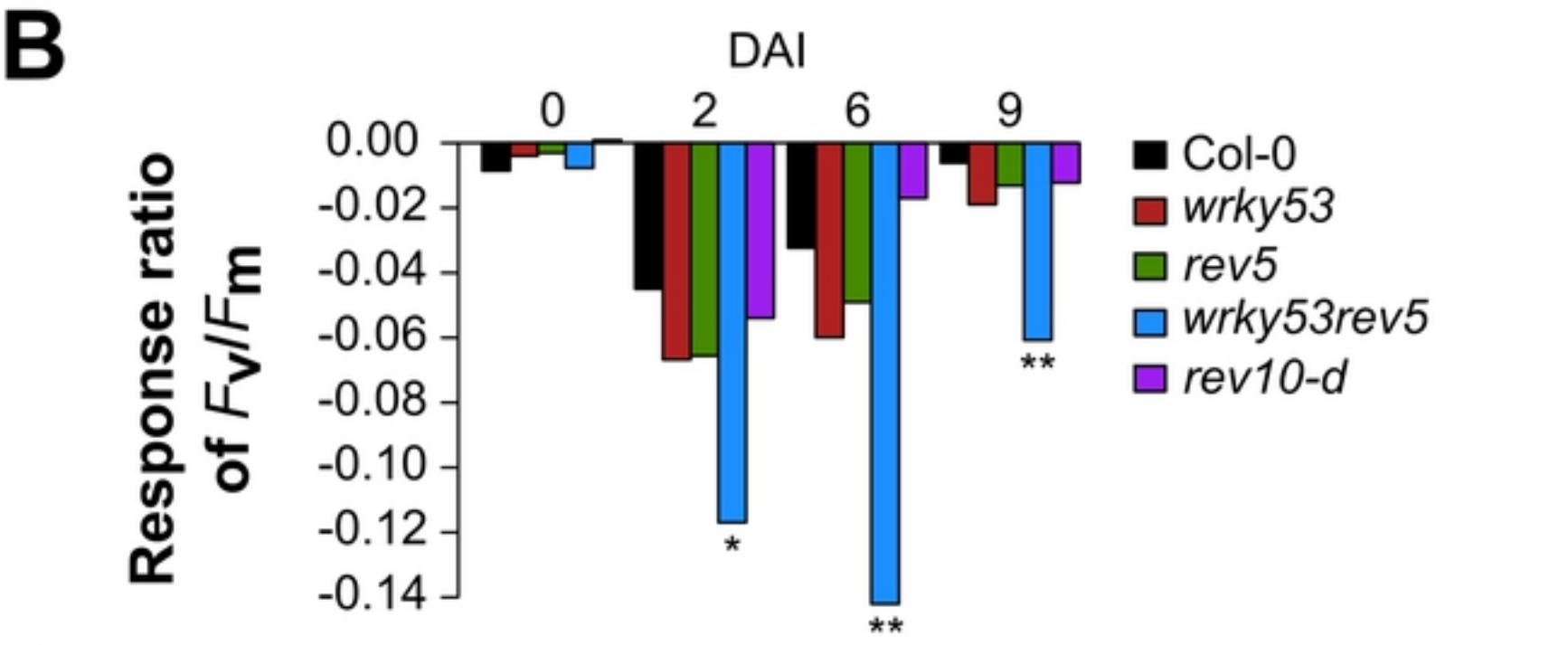

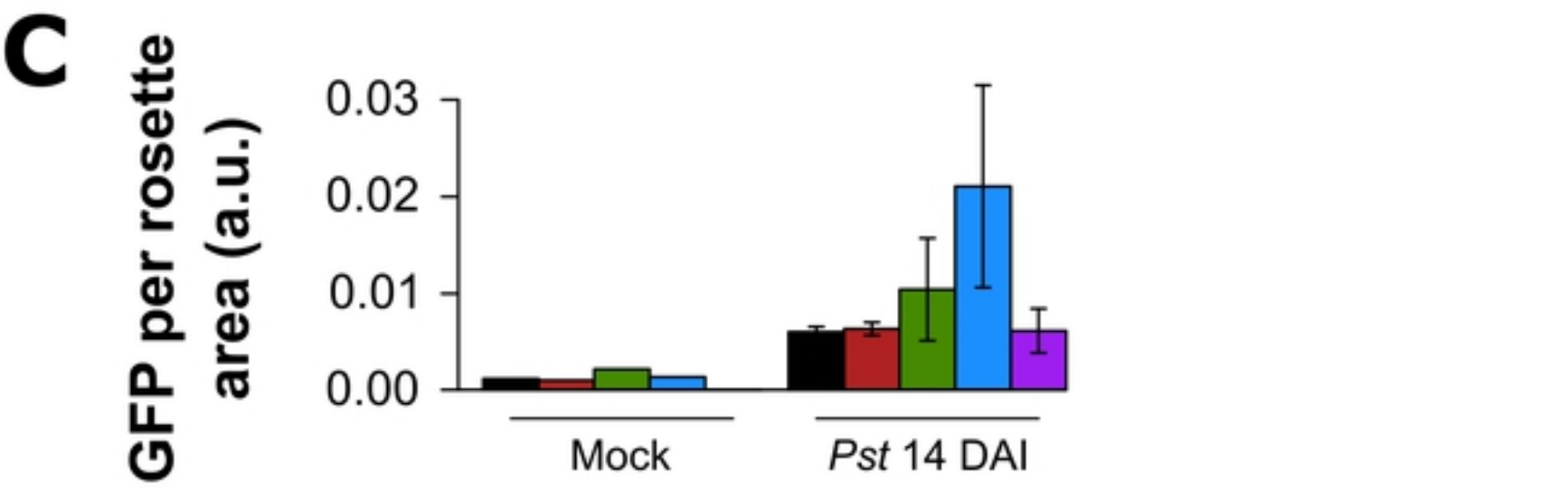

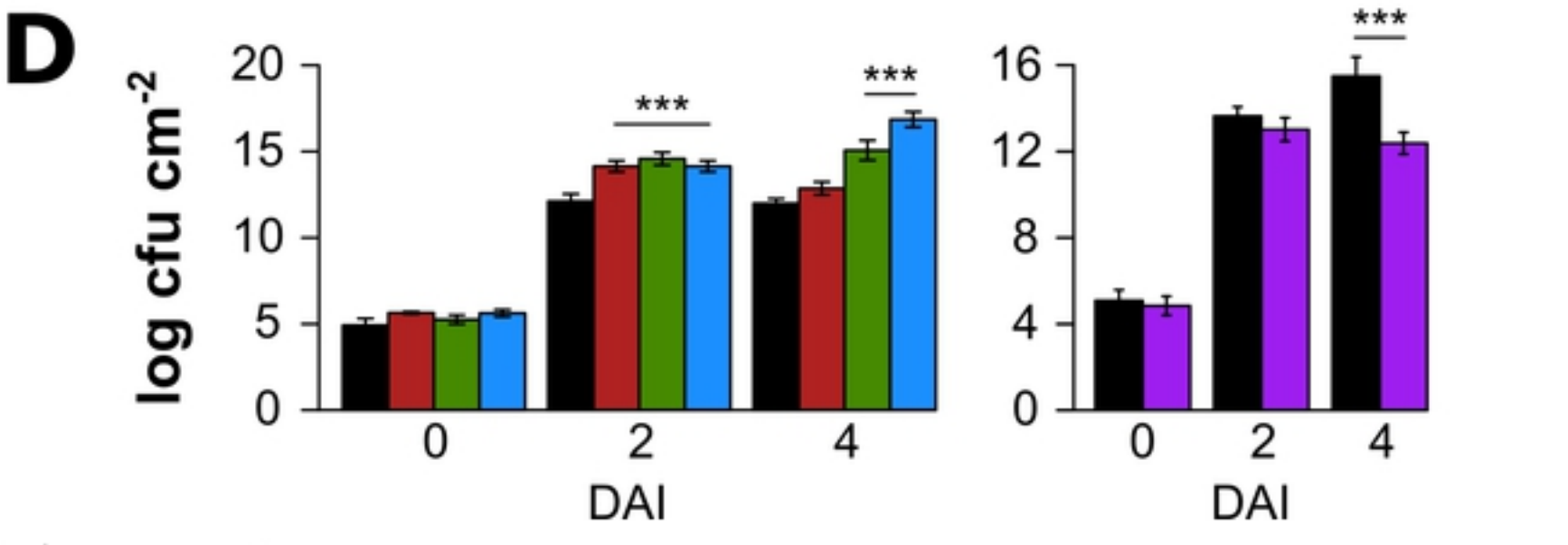

Figure 5

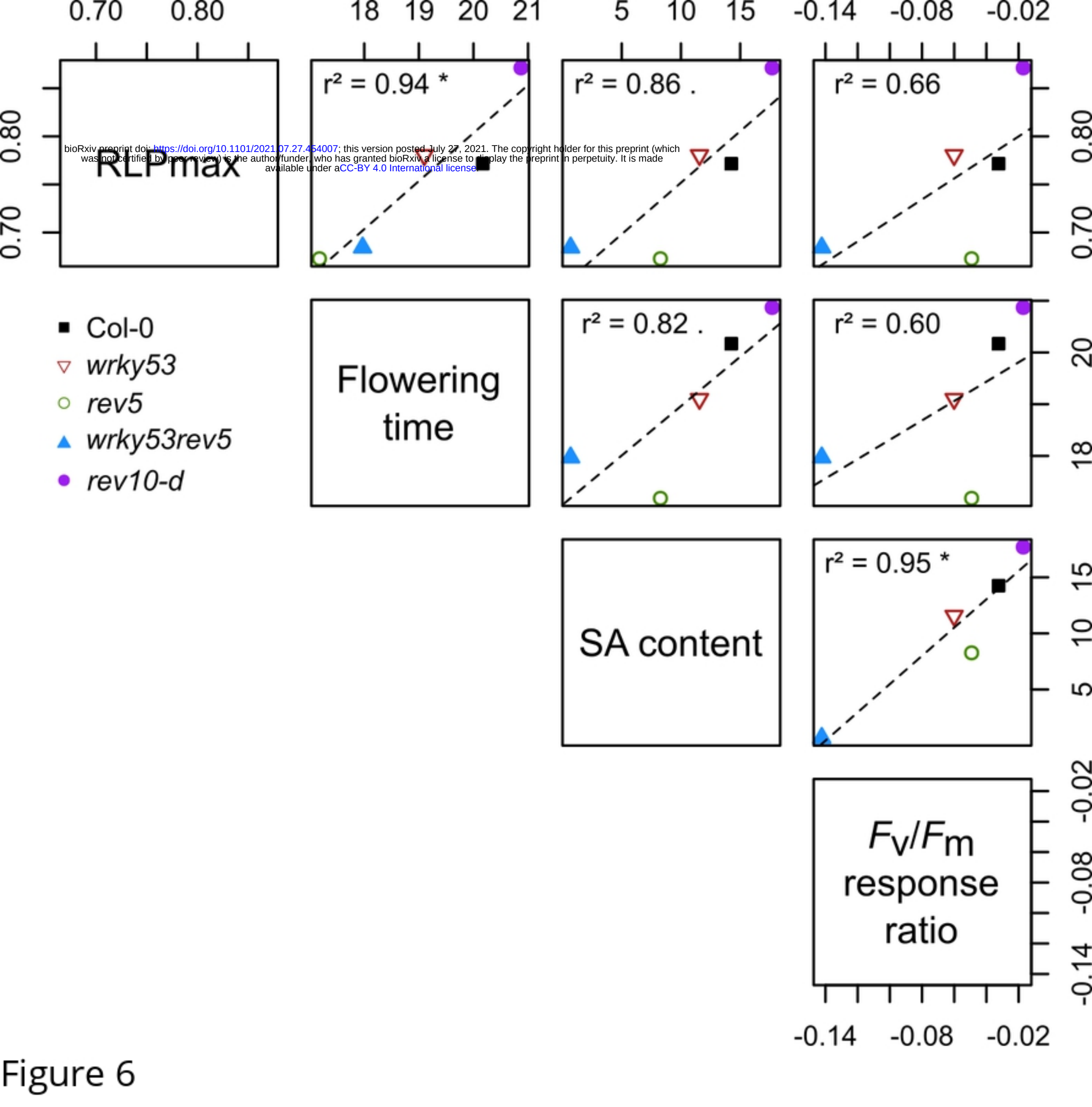

Figure 6